Effective coating of titania nanoparticles with alumina via atomic layer deposition

Azizpour, H.; Talebi, M.; Tichelaar, F. D.; Sotudeh-Gharebagh, R; Guo, J.; van Ommen, J. R.; Mostoufi, N

DOI
10.1016/j.apsusc.2017.07.168

Publication date
2017

Document Version
Final published version

Published in
Applied Surface Science

Applied Surface Science 426 (2017) 480–496

Contents lists available at ScienceDirect

Applied Surface Science

journal homepage: www.elsevier.com/locate/apsusc

Full Length Article

Effective coating of titania nanoparticles with alumina via atomic layer deposition

H. Azizpour[a], M. Talebi[b], F.D. Tichelaar[c], R. Sotudeh-Gharebagh[a], J. Guo[d], J.R. van Ommen[b,*], N. Mostoufi[a,*]

[a] Multiphase Systems Research Lab., School of Chemical Engineering, College of Engineering, University of Tehran, P.O. Box 11155/4563, Tehran, Iran
[b] Delft University of Technology, Faculty of Applied Science, van der Maasweg 9, 2629 HZ, Delft, The Netherlands
[c] Delft University of Technology, Kavli Institute of Nanoscience, National Centre for HREM, Lorentzweg 1, 2628 CJ, Delft, The Netherlands
[d] Multi-Phase Mass Transfer & Reaction Engineering Lab, College of Chemical Engineering, Sichuan University, Chengdu 610065, China

ARTICLE INFO

Article history:
Received 13 April 2017
Received in revised form 30 June 2017
Accepted 19 July 2017
Available online 23 July 2017

Keywords:
Atomic layer deposition
Growth per cycle
Oxidizer
Photocatalytic activity
Coating of titania

ABSTRACT

Alumina films were deposited on titania nanoparticles via atomic layer deposition (ALD) in a fluidized bed reactor at 180 °C and 1 bar. Online mass spectrometry was used for real time monitoring of effluent gases from the reactor during each reaction cycle in order to determine the optimal dosing time of precursors. Different oxygen sources were used to see which oxygen source, in combination with trimethyl aluminium (TMA), provides the highest alumina growth per cycle (GPC). Experiments were carried out in 4, 7 and 10 cycles using the optimal dosing time of precursors. Several characterization methods, such as high resolution transmission electron microscopy (HRTEM), Brunauer-Emmett-Teller (BET), energy dispersive X-ray spectroscopy (EDX), Fourier transform infrared (FTIR), X-ray diffraction (XRD) and instrumental neutron activation analysis (INAA), were conducted on the products. Formation of the alumina film was confirmed by EDX mapping and EDX line profiling, FTIR and TEM. When using either water or deuterium oxide as the oxygen source, the thickness of the alumina film was greater than that of ozone. The average GPC measured by TEM for the ALD of TMA with water, deuterium oxide and ozone was about 0.16 nm, 0.15 nm and 0.11 nm, respectively. The average GPC calculated using the mass fraction of aluminum from INAA was close to those measured from TEM images. Excess amounts of precursors lead to a higher average growth of alumina film per cycle due to insufficient purging time. XRD analysis demonstrated that amorphous alumina was coated on titania nanoparticles. This amorphous layer was easily distinguished from the crystalline core in the TEM images. Decrease in the photocatalytic activity of titania nanoparticles after alumina coating was confirmed by measuring degradation of Rhodamine B by ultraviolet irradiation.

1. Introduction

Functionalization of the surface of nanoparticles is needed in many industrial applications [1–3]. Applying an inert film to shield the surface of nanoparticles for avoiding spontaneous interaction of the core powder with its surrounding material is an example of these applications [1,2,4,5], for instance, deposition of alumina and silica on titania nanoparticles for decreasing unfavorable photo activity effects of titania [5–7]. Titania nanoparticles, as white pigment, is the prevalent material used in paints, plastics and ultraviolet (UV) blockers in sunscreens [1,2,8–10]. However, titania is a well-known photocatalyst that facilitates the oxidation of organic compounds which degrades the polymer surrounding the pigment in paints or can adversely affect the skin when used in sunscreens [2,6,8–11]. In order to solve these problems, the photocatalytic activity of titania nanoparticles must be quenched and coating an ultrathin inactive film on the surface of titania particles can be proposed to decrease the photoactivity of the nanoparticles [2,6–13].

Atomic layer deposition (ALD) is a chemical technique suitable for depositing thin layers, with precise control of the thickness, on the surface of nanoparticles [14,15]. This technique offers the possibility of coating of primary particles as well as complex nanostructures with high surface area [1,16–21]. Researchers from the former Soviet Union were the first to establish ALD principle, but referred to it as molecular layering [3,18]. The ALD process can be

* Corresponding authors.
E-mail addresses: J.R.vanOmmen@tudelft.nl (J.R. van Ommen), mostoufi@ut.ac.ir (N. Mostoufi).

http://dx.doi.org/10.1016/j.apsusc.2017.07.168
0169-4332/

Nomenclature

a_c	specific surface area of particles (m^2/g)
C_A	concentration of precursor (mol/m^3)
C/C_0	relative concentration of RhB
F_{TMA}	molar flow rate of TMA (mol/min)
$n_{activesite}$	number of active sites ($1/nm^2$)
P^*_A	vapor pressure of precursor (Pa)
Q_i	flow rate of inert gas (m^3/min)
S_{BET}	specific surface area (m^2g^{-1})
T	temperature (K)
$V^{1p}_{Al_2O_3}$	volume of aluminum oxide in each particle (m^3)
x_{Al}	mass fraction of aluminum

Greek letters

δ	thickness of alumina layer (nm)
ρ	density of the material ($g\,cm^{-3}$)

described as two complementary and self-limiting gas-solid reactions, applied in a sequential way to build-up solid layers on the material surface [1,8–11,16–20,22–30]. In the first step, a reactant is adsorbed on the surface of the substrate by a self-terminating reaction. In the second step, a purge gas removes gaseous by-products from the reactor to prevent progress of unwanted reactions in the gas-phase between injections of precursors. In the third step, the second precursor reacts with the adsorbed monolayer. Finally, in the fourth step, a purge gas discharges the by-product gases from the reactor again [1,8–11,16–20,22–30]. These steps, called a cycle of the ALD process, can be repeated as many times as required to obtain the desired thickness of the film deposited on the particle [1,16–20,31].

It is important to eliminate radial and axial concentration gradients in the ALD reactor to achieve a high quality product. Therefore, fluidized bed reactors, which can provide an efficient contact between fluid and solids, are well suited for large scale ALD operations [1,8,22,32–41]. High transport rates in fluidized beds can be used in the ALD process to produce uniform products that is often hard to achieve in other types of reactors. Ferguson et al. [42–45] showed that ALD has the capacity of coating thin films on the surface of primary particles. Miikkulainen [46], Puurunen [18] and George [23] reviewed advances in ALD and highlighted the combination of different materials that can be applied for this process. Puurunen [18] described in details mechanism of the widely studied trimethyl aluminium (TMA)-water system. Coating of alumina on particles by ALD in a fluidized bed was utilized for forming a barrier against oxidation and other applications [2,5,47–51]. It was found that coating of $LiMn_2O_4$ cathode particles with alumina film increases the lifetime of Li-ion batteries [22,52].

The ALD coating of alumina on a variety of powders has been investigated at different operating conditions, from vacuum to atmospheric, and different temperatures, ranging from 25 to ~180 °C [2,4,18,19,22,52–62]. Most researchers [2,9,11,19,22,27,52,62,63] have utilized water as the oxygen source in ALD of TMA for alumina coating. However, water tends to form hydrogen bonds on the surface of oxide powders which makes its removal difficult during the purging step [58]. Desorption of ozone from surface of the substrate requires shorter purging time as compared with water. Thus, using ozone as the oxidizer can be advantageous. Using ozone and other oxygen sources (water and deuterium oxide) in the ALD of TMA for alumina coating has been investigated in some types of reactors [58,59,64–66] but not in fluidized beds.

The aim of the present work is to experimentally investigate the ALD of aluminum oxide on titania nanoparticles at 1 bar and 160–180 °C. Online mass spectrometry is used for real time monitoring of reactants and gaseous products throughout the ALD reaction. Deuterium oxide (D_2O) was used instead of water to distinguish, in the mass spectrum, between the methane molecules formed by the ALD reactions and those formed directly from fragmentation of TMA in the mass spectrometer. The effect of different oxygen sources (water, deuterium oxide and ozone) on the alumina ALD with TMA is studied in terms of GPC, conformity and saturating dosing time. Also, the influence of alumina coating on the photocatalytic behavior of titania core powder is investigated.

2. Experimental section

2.1. Experimental setup

ALD of alumina on titania nanoparticles was performed in a vibrated fluidizing bed reactor at 1 bar. Schematic of the set-up is shown in Fig. 1. The reactor was made of glass with an internal diameter of 26 mm and height of 500 mm. In each test, the reactor was initially filled with 2.5 gr of titania nanoparticles. The reactor was placed on a vertical vibrating table with two vibromotors in order to vibrate the reactor with a frequency of 35 Hz to assist the fluidization of powder [19]. The reactor temperature was kept in the range of 160–180 °C by means of an infrared lamp positioned parallel to the column. A thermocouple was placed inside the bed to control the reactor temperature. The temperature range was within the preferred ALD growth window of alumina [19,58]. Nitrogen with a flow rate of 0.5 L/min was introduced to the column through a porous plate distributor with a pore size of 37 μm. To evacuate unreacted TMA and byproducts, the exhaust gases were led through separate gas washers filled with Kaydol oil. The whole setup was placed in a cabinet filled with nitrogen.

Aeroxide P25 titanium oxide (TiO_2) particles from Evonik Industries (Hanau, Germany), which are mainly non-porous with specific surface area of 51 m^2/g, were utilized as nanoparticles in the experiments. TMA was supplied by Akzo Nobel HPMO (Amersfoort, The Netherlands) in a 600 mL WW-600 stainless steel bubbler and was kept at 30 °C. Three different oxidizers were used in this research, including demineralized water, deuterium oxide and ozone. Distilled water and deuterium oxide were kept in a similar bubbler. Ozone was produced by an ozone generator (OAS Topzone).

2.2. Experimental procedure

2.2.1. Coating experiments

Online mass spectrometry was used to monitor the reaction progress during each ALD cycle and to tune the optimum usage of precursor in the minimum processing time and minimize excess usage of precursors. Required dosing time for saturation of titania nanoparticles for three sets of experiments with [(TMA-H_2O); (TMA-D_2O); (TMA-O_3)] was determined with online mass spectrometry from breakthrough of precursor. The experiments were performed in 4, 7 and 10 cycles. The self-limiting nature of ALD reaction was checked by increasing the dosing time of precursors. Deposition of alumina was carried out with increasing the dosing time of precursors in a separate set of experiments. Excess deuterium oxide was applied as the oxidizer in experiments and 4, 7 and 10 cycles were performed with establishing a feeding sequence of TMA–N_2–D_2O—N_2 (30–7–30–7 min). This translates into dosing of TMA at 10 times the ideal dosing time of precursors and purging the system with N_2 for 7 min (which corresponds to 13 residence times). Results of this set of experiments were compared with those obtained by applying the optimal dosing time determined by online monitoring of effluent gases via mass spectrometry. This compar-

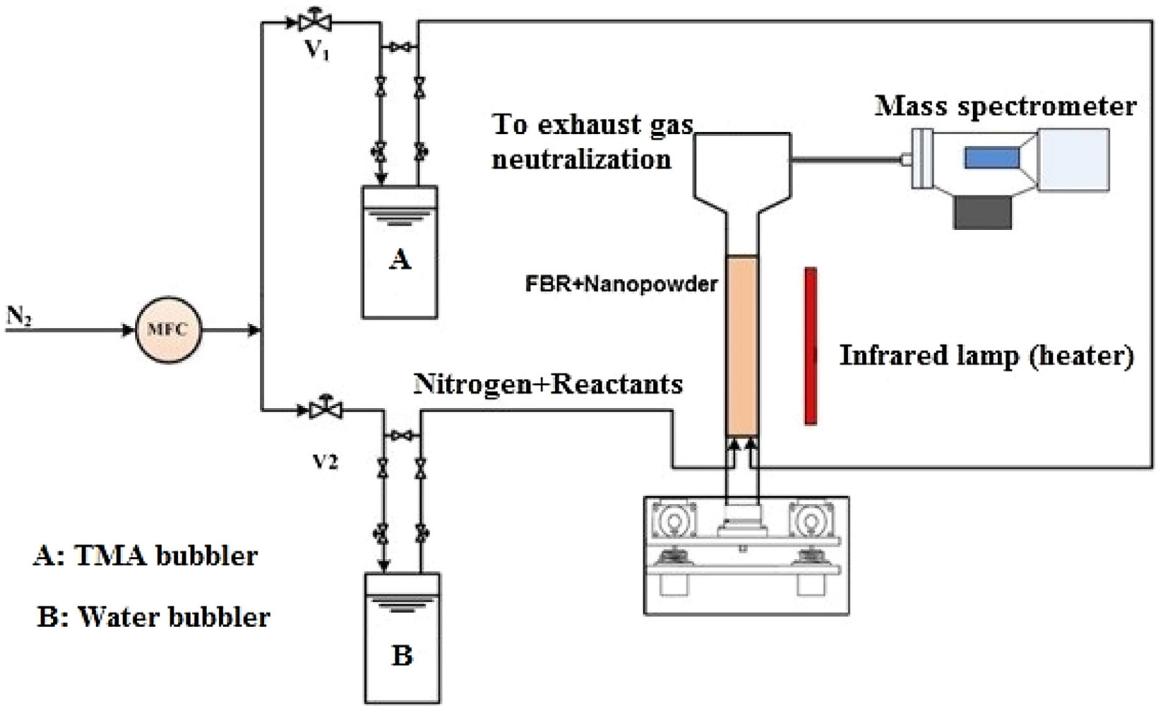

Fig. 1. Schematic of the ALD fluidized bed reactor.

ison is important for checking if the purging time is sufficient to obtain a desired film.

2.2.2. Photocatalytic tests

The photocatalytic activity of coated nano-powders were determined by using the degradation of Rhodamine B (RhB) under UV light. In each test, 30 mg of the powders were added to 30 mL RhB solution (8 mg/L) and continuously mixed by a magnetic stirrer in the dark for 30 min to obtain adsorption/desorption balance and get a uniform suspension. The suspension was then exposed to UV radiation generated by a 45 W mercury lamp for various exposure times. The solution was then analyzed by the UV–visible spectrophotometry technique to determine the residual concentration of RhB in the solution.

2.3. Characterization of the coating

2.3.1. X-ray diffraction

X-ray diffraction (XRD) analyses were performed in Bragg Brentano geometry, using a Bruker AXS D8 Advance diffractometer with Lynx Eye detector. The scans were recorded using a Co Kα source for 2θ range between 5 and 95° with a step size of 0.025°.

2.3.2. Transmission electron microscopy

Transmission electron microscopy (TEM) was performed using a FEI Tecnai TF20UT/STEM operating at 200 kV and a FEI Cs corrected cubed Titan operating at 300 kV in order to determine the thickness of alumina film deposited on titania particles. The powder was dispersed in ethanol, ultra-sonically shaken for two minutes and a droplet was put on a Quantifoil carbon foil on a Cu grid using a pipette. High resolution images were obtained as well as Annular Dark Field (ADF) images in Scanning TEM mode (STEM). Energy Dispersive X-ray (EDX) measurements were done using an Oxford Instruments X-Max^N 100TLE detector. STEM mode was used to obtain elemental maps by collected an EDX spectrum for each position of the electron beam in the scanned area.

2.3.3. BET surface area

The specific surface of coated particles was determined by the Brunauer-Emmet-Teller (BET) test. Isotherms of N_2 adsorption–desorption were measured with a Micrometrics TriStar II 3020 based on acquisition of N_2 adsorption isotherm at 77 K in relative pressure 0.008 – 0.98. Pre-treatment was carried out by purging of powder with dry nitrogen at 423 K for 16 h.

2.3.4. FT-IR spectroscopy

Fourier transform infrared (FTIR) spectroscopy was used to determine the fundamental vibrations of the material in the range of 4000–400 cm^{-1} (mid-infrared). FTIR provides information about the chemical bonds in the sample. The FTIR spectra were recorded on a Thermo Scientific Nicolet 8700 FTIR spectrometer equipped with a DTGS-detector and a high-temperature DRIFT-cell with CaF_2 windows (HVC Harrick Praying Mantis). The samples were first dried at 150 °C. The spectrum of each sample was determined by accumulating 128 scans at a resolution of 4 cm^{-1}, under a 20 mL/min flow of helium.

2.3.5. Instrumental neutron activation analysis

Instrumental neutron activation analysis (INAA) is a multi-element analytical technique used for both qualitative and quantitative analysis of elements. To carry out this analysis, the specimen was placed into a nuclear reactor and irradiated with neutrons, leading to formation of radioisotopes of the elements. Following irradiation, decay of radioisotopes was detected via the emission of particles, or more importantly γ-rays, which are characteristic of the elements. This technique was applied to determine the mass fraction of aluminum and other elements in the coated samples. Using the mass fraction of aluminum in the samples and assuming substrate particles to be spherical, the volume of aluminum oxide in each particle and the film thickness was calculated by the equation suggested by Valdesueiro et al. [19]. In the calculation of film thickness, the density of aluminum oxide at 170 °C and its Sauter mean diameter were considered to be 3000± 200 kg/m^3 and of 32.7 ± 3.3 nm, respectively [19].

3. Results and discussion

3.1. Mass spectrometry

3.1.1. TMA-water

Precursor efficiency is critical for the economic feasibility of ALD of nanoparticles due to the relatively large amount of reactants needed [17,67]. Therefore, determining the optimum usage of precursor during coating is necessary. Online mass spectrometry was used to carry out residual gas analysis during deposition of alumina on titania particles. Useful information can be obtained by analyzing the mass spectrometry data during an ALD cycle. Fig. 2 shows the residual gas composition gathered throughout the second cycle of alumina coating on titania nanoparticles, using TMA and water. During the deposition, primary and fragmentation peak of the reaction products and precursor molecules were monitored online through mass spectrometry. The monitored m/z peaks during exposure of TMA and water can be seen in Table S1 (Supplementary Information S1). In this table, the entire molecules and their fragments, derived through ionization of their parent molecule, are shown. Alumina ALD using TMA and water occurs according to the following two subsequent reactions, in which ‖ designates the surface species [11,12,27,42,54].

$$\| - \mathrm{AlOH} + \mathrm{Al(CH_3)_3} \rightarrow \| - \mathrm{AlOAl(CH_3)_2} + \mathrm{CH_4} \quad (1)$$

$$\| - \mathrm{AlOAl(CH_3)_2} + 2\mathrm{H_2O} \rightarrow \| - \mathrm{AlOAl(OH)_2} + 2\mathrm{CH_4} \quad (2)$$

During each half cycle, the reactants completely saturate the active sites on the surface of powder, making ALD a self-limiting process [2,8,19,22]. Alumina deposition ALD using TMA and water is based on the following reaction [11,42,68]:

$$2\mathrm{Al(CH_3)_3} + 3\mathrm{H_2O} \rightarrow \mathrm{Al_2O_3} + 6\mathrm{CH_4} \quad (3)$$

It can be seen in Fig. 2 that at the beginning, there is a sudden increase in the methane signal as the precursor (TMA) is fed into the reactor. This methane signal is related to the product of reaction (1). When the reaction becomes near complete throughout the bed, methane generation begins to decrease and a breakthrough of fragmentation products of TMA is observed. With an increase in the TMA signal, the methane signal also increases due to TMA decomposition in filament of the mass spectrometry. Furthermore, a break point in the mass spectrum of methane, which separates two sources of methane, takes place close to the TMA breakthrough. This breakpoint has been specified in Fig. 2. In fact, the signals of fragmentation products of TMA do not increase until the methane signal due to reaction has dropped. Since decomposition of the precursor in the filament produces small amounts of methane, the methane increases and its signal does not return to its base level. Intensity of the signal of fragmentation products of TMA (m/z = 42) remains constant with more feeding of TMA into the reactor. The reactor is then purged after the breakthrough to remove the reaction products and unreacted precursor from the reactor. As a result, the methane signal returns to its base level. In the second half cycle, water is fed into the reactor, leading to a sudden increase in the methane signal according to reaction (2). After a while, the methane signal decreases and the breakthrough of fragmentation products of water can be observed, indicating saturation of the surface with water. The water breakthrough does not take place at the maximum of methane signal and does not increase until the methane signal is considerably dropped. Similar results were obtained for alumina coating on iron (II, III) oxide (Fe_3O_4) nanoparticles [4] and also for a large batch of micron-sized metal particles using online mass spectrometry [9]. In each half-reaction, a gas precursor reacts with a functional group on the surface and forms methane as a by-product. This surface reaction continues until all available surface functional groups are reacted [9]. Similar plot and trend were obtained for other reaction cycles as can be seen in Fig. S1 (Supplementary Information S1). Logarithmic scales have been used for vertical axis (ion current) to better illustrate the mass spectrometry data.

To determine the precursor dosing time, the total required moles of precursor for saturation of the surface of substrate and molar flow rate of precursor should be calculated. The required moles of precursor for saturation of the surface of substrate can be estimated from the total amount of active sites in the bed of particles (i.e., number of hydroxyl groups divided by the Avogadro number). The molar flow rate of the precursor can be calculated from:

$$F_A = C_A Q_{A,in} = Q_{A,in}\left(\frac{P^*_A}{RT}\right) \quad (4)$$

where C_A is the concentration of precursor (mol/m^3), P^*_A is the vapor pressure of precursor at bubbler temperature (Pa) and $Q_{A,in}$ is the flow rate of inert gas through the bubbler (m^3/min). Thus, the ideal dosing time of the precursor in each ALD cycle can be estimated from the required mole of precursor for surface saturation divided by the molar flow rate of the precursor:

$$t_{idealofTMA} = \frac{\left(\frac{m a_c n_{activesite}}{N_A}\right)}{F_{TMA}} \quad (5)$$

where a_c is the specific surface area of TiO_2 nanoparticles (51 m^2/g), m is the mass of powder placed inside the column (2.50 g) and $n_{activesite}$ is the surface concentration of hydroxyl groups (5.0 OH/nm^2). The flow rate of nitrogen (0.5 L/min) as well as TMA bubbler temperature (30 °C) and water bubbler temperature (10 °C) were considered for calculating the molar flow rate of precursors. According to the overall reaction of TMA and water (reaction 3), required moles of water for saturation of the surface is 1.5 times moles of TMA. Thus, the ideal dosing time of water can be calculated from:

$$t_{idealofwater} = 1.5\frac{\left(\frac{m a_c n_{activesite}}{N_A}\right)}{F_{water}} \quad (6)$$

According to Eqs. (5) and (6), the ideal dosing time of TMA and water are about 2.63 min and 6.3 min, respectively, at the conditions of this work. These times are in reasonable agreement with the time of breakpoint (2.6 min) as well as breakthrough times of TMA (~2 min) and water (~7.2 min) determined from the mass spectrum (Fig. 2).

3.1.2. TMA- deuterium oxide

Alumina ALD using TMA and deuterium oxide occurs according to the two subsequent reactions [69], in which ‖ indicates the surface species:

$$x\| - \mathrm{AlOD} + \mathrm{Al(CH_3)_3} \rightarrow \| - \mathrm{AlO}_x\mathrm{Al(CH_3)}_{3-x} + x\mathrm{CH_3D} \quad (7)$$

$$\| - \mathrm{AlO}_x\mathrm{Al(CH_3)}_{3-x} + 1.5\mathrm{D_2O} \rightarrow \| - \mathrm{AlO}_x\mathrm{AlO}_{(3-2x)/2}(\mathrm{OD})_x + (3-x)\,\mathrm{CH_3D} \quad (8)$$

Deuterium oxide (D_2O) was used instead of water to distinguish, in the mass spectrum, between the methane molecules formed by the ALD reactions and the methane molecules formed directly from the fragmentation of TMA in the mass spectrometer. Fig. 3 shows the residual gas analysis gathered throughout the first alumina coating cycle (using TMA and deuterium oxide) on titania nanoparticles. Primary and fragmentation peak of reaction products and precursor molecules were monitored online through the mass spectrometry. The monitored m/z peaks of the entire molecules and their fragments during exposure of TMA and deuterium oxide are given in Table S2 (Supplementary Information S2).

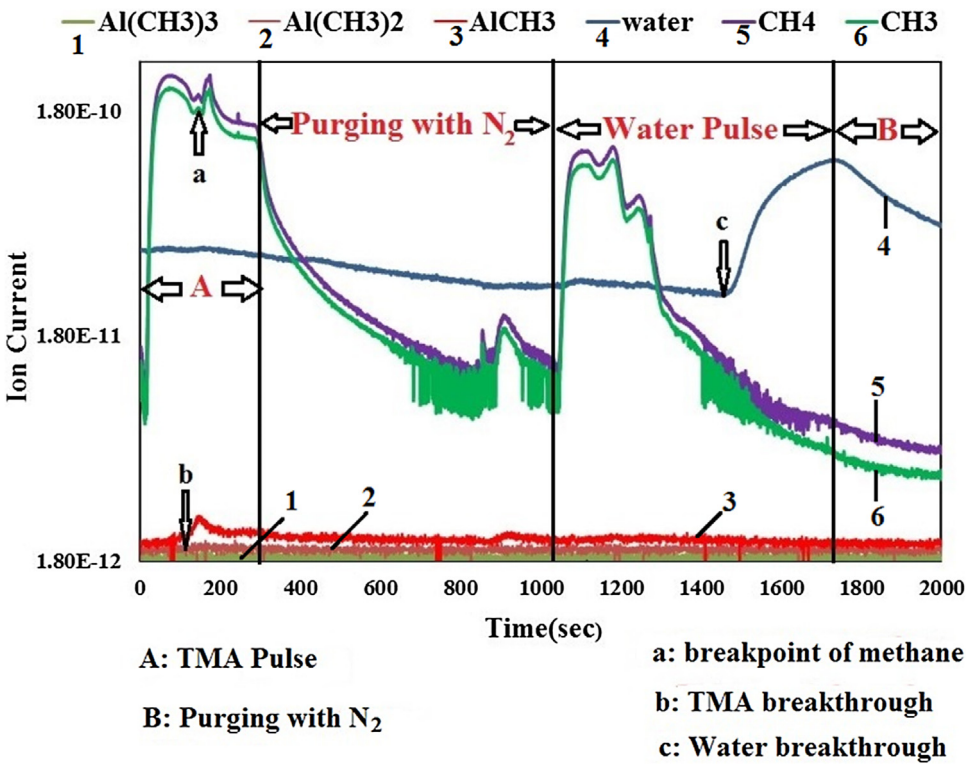

Fig. 2. Mass spectrum of TMA-H_2O ALD on TiO_2 P25 during cycle 2.

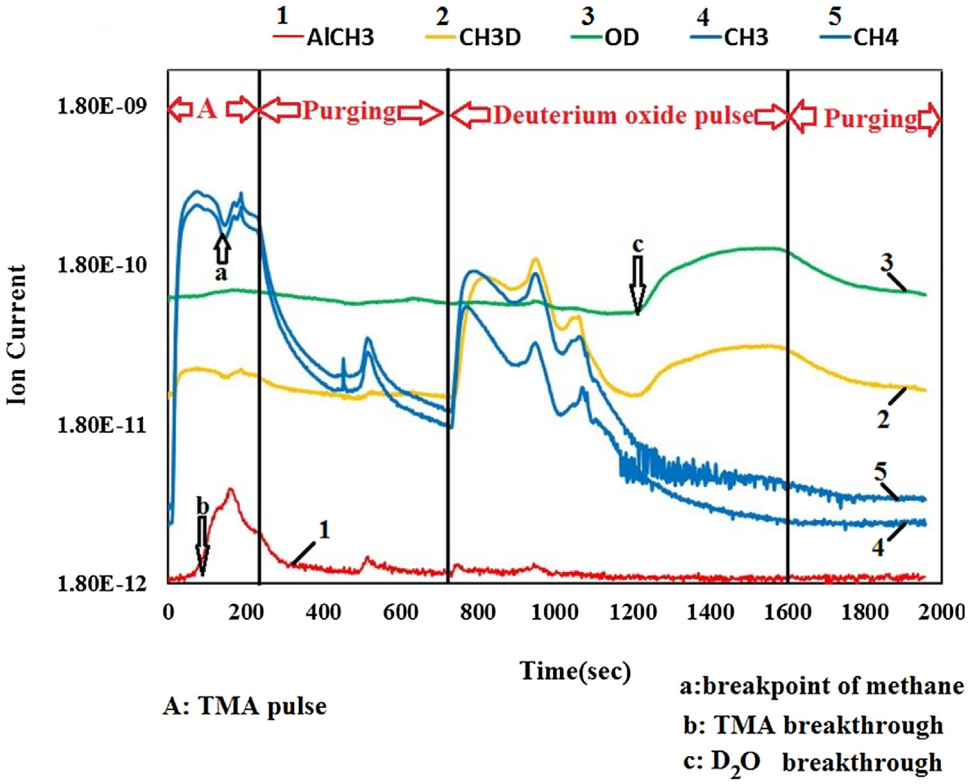

Fig. 3. Mass spectrum of TMA-D2O on TiO2 P25 during cycle 1.

The peaks at $m/z = 42$, 57 and 72 are associated with the fragmentation of the precursor molecule in the mass spectrometry filament and can be related to the concentration of TMA at the outlet of the reactor. Also, the peak at 17 corresponds to CH_3D in the fragmentation product which is the main product of the half reactions (7) and (8).

Fig. 3 shows a sudden increase in the methane signal as the precursor (TMA) is fed to the reactor. This corresponds to the pro-

duction of methane due to the reaction between TMA and hydroxyl groups on the surface of particles. Soon after the generated methane begins to decrease and breakthrough of the fragmentation products of TMA is observed, saturation of substrate surface occurs (arrows indicate the breakthrough of TMA and deuterium oxide in Figs. 3 and 4). With more flow of TMA, the methane signal also increases because of direct formation of methane due to the fragmentation of TMA in the mass spectrometer. Since decomposition of the precursor produces small amounts of methane, the methane signal does not return to its base level. Breakthrough of the precursor takes place close to the break point of the methane signal. The signal corresponding to products of fragmentation of TMA remain constant with more feeding of TMA to the reactor. Since there was no deuterium before initial dosing of D_2O into the reactor, an instantaneous increase of the signal of CH_3D byproduct was not seen.

After enough purging, the methane signal returns to its base level and D_2O was fed into the reactor. D_2O reacts with the adsorbed monolayer during the second half of the reaction and CH_3D and CH_4 signals increase instantaneously. As dosing of D_2O proceeded, CH_3D and CH_4 signals began to decrease and the breakthrough of fragmentation products of deuterium oxide was observed, indicating saturation of the substrate surface with oxidizer molecules. Similar to water breakthrough, the D_2O breakthrough does not take place at the maximum of the product signal (here, CH_3D) and does not increases until the CH_3D signal has considerably dropped. The signal of D_2O appeared after about 8 min of D_2O dosing (arrows indicate the breakthrough of TMA and deuterium oxide in Figs. 3 and 4). At this point, the surface reaction was nearly complete and nitrogen was fed into the reactor to purge any residual reaction products or unreacted D_2O from the reactor. Similar results were reported by King et al. [1] for online mass spectrometry of ALD of Al_2O_3 on 16 μm high density polyethylene (HDPE) particles at 77 °C.

The ideal dosing times of TMA and D_2O can be calculated by considering the surface area of TiO_2 particles (51 m^2/g), the mass of powder placed inside the column (2.5 g) and the flow rate of nitrogen (0.5 L/min.) as well as TMA bubbler temperature (30 °C) and D_2O bubbler temperature (10 °C). The vapor pressure of deuterium oxide is 1000 Pa at 10 °C [70]. The ideal dosing times were calculated based on Eqs. (5) and (6) to be about 2.66 min for TMA and 7.8 min for D_2O in the conditions of this work. These times are in reasonable agreement with the time of breakpoint of methane signal (2.5 min) as well as breakthrough times of TMA (~1.6 min) and D_2O breakthrough (~8.3 min) determined from the mass spectra (Figs. 3 and 4).

Analysis of the residual gas, carried out throughout the second cycle of coating, is shown in Fig. 4. Since the particle surface was saturated with OD groups at the end of the previous cycle, an instantaneous increase in the peak of CH_3D can be observed with dosing of TMA in the second cycle. As the dosing of TMA proceeded, CH_3D as well as the corresponding signal decreased and the signal of TMA fragmentation appeared after 2 min. (TMA breakthrough). As can be seen in Fig. 4, the time of TMA breakthrough takes places close to the time of break point of methane. Definition of the break point becomes important when the peak of TMA is not sharp enough and detecting TMA breakthrough is not possible. Therefore, the time of occurrence of this break point can be considered as the time of saturation of surface with TMA. After enough purging, D_2O was dosed into the reactor and again a sharp increase in the CH_3D signal was observed. As the D_2O dosing proceeded, signals of CH_3D and CH_4 began to decrease and the signal of D_2O appeared after about 8.0 min of D_2O dosing. As reported by Juppo et al. [69], the increase in the CH_4 signal during the early stage of D_2O pulse and also the increase in the CH_3D intensity at D_2O breakthrough can be related to the effect of neighboring peaks. On the other hand, during the D_2O pulse, OD^+ (m/e=18) is produced and can contribute to the peak of CH_3D (m/e=17). In the case of increase of methane, CH_3D and its fragments can cause the same effect on CH_4^+ (m/e=16).

The same phenomena were observed in the reaction of TMA-D_2O on 2 gr of micron sized γ-alumina (60 m^2/gr) and the flow rate of nitrogen (0.75 L/min.). Fig. S2 (Supplementary Information S2) shows all fragments of this ALD reaction for 4 cycles. For easier interpretation of the results, the fragments are shown in separate figures (Figs. S2(a-c)). The trends for all products and oxidizer fragments in the coating of alumina on micron sized particles are the similar as that for nanoparticles. Unlike the mass spectrum of reaction of TMA and deuterium oxide with TiO_2 nanoparticles, changes in TMA fragments is not clear in case of reaction with γ-alumina. However, since the breakthrough of TMA occurred close to the maximum fragmentation of methane, this maximum was considered for determining the optimum dosing time of TMA. The ideal dosing times estimated from Eqs. (4) and (5) are about 1.66 min for TMA and 4.5 min for D_2O at the conditions of this work. The results are rather close to the breakthroughs in the mass spectrum which are 2.4 min and 3.85 min for TMA and oxidizer saturation, respectively.

The same phenomena can be seen in the reaction of TMA-D_2O on silica gel powder with large surface area. The ideal dosing times of the precursors can be calculated by taking into account the surface area of silica gel powder (520 m^2/g), the mass of powder placed inside the column (1.0 g), the flow rate of nitrogen through TMA and D_2O bubblers were set to 0.5 L/min. and 1.0 L/min., respectively. Ideal dosing times estimated by this method are about 10.5 min for TMA and 16.0 min for D_2O. These times are close to those obtained from the saturation time determined from the break point of methane signal which is about 8.5 min for TMA and breakthrough times of D_2O which is about 20 min. It should be noted that although the intensity of breakthrough of TMA in coating of alumina on micron sized particles is not as clear as in nanoparticles, this breakthrough (or optimum dosing time of TMA) can be determined based on the time of breaking point of the methane signal in mass spectrum of methane fragments. As mentioned in the previous section, this point corresponds to the breakthrough of TMA in the coating of nanoparticles, thus, can be used for determining of TMA breakthrough. This point is shown with arrows in Figs. 4 and 5. Also, the mass spectrum of the second cycle can be seen in Fig. S3 (Supplementary Information S2).

Using deuterium oxide instead of water in alumina ALD lead to distinguish between the methane molecules formed by the ALD reactions and the methane molecules formed directly from the fragmentation of TMA in the mass spectrometer. Also, the D_2O breakthrough does not take place at the maximum of the product signal and increases until the product signal has considerably dropped (Similar to water breakthrough).

3.1.3. TMA-Ozone

Fig. 6 shows the analysis of the residual gas gathered throughout the first cycle of alumina coating on titania nanoparticles, using TMA and ozone. The mechanism of growth of alumina film with TMA and ozone is different from TMA and water or deuterium oxide. The first half of the ALD reaction of TMA-ozone (reaction of TMA with active sites) is the same as reaction (1). However, the reaction in the second half cycle occurs as follows, in which ‖ indicates the surface species [59]:

$$\begin{aligned} &\| - \mathrm{AlOAl(CH_3)_2} \xrightarrow{O_3} \| - \mathrm{AlOAl(OCH_3)_2}\,(\textit{metoxy}) \xrightarrow{-CH_4} \| \\ &-\mathrm{AlOAlOCHO}\,(\textit{formate}) \xrightarrow{O_3} \| - \mathrm{AlOAlOCOOH}\,(\textit{Carbonate}) \xrightarrow{-CO_2} \| \\ &-\mathrm{AlOAl(OH)_2}\,(\textit{hydoxyls}\quad \textit{group}) \end{aligned} \tag{9}$$

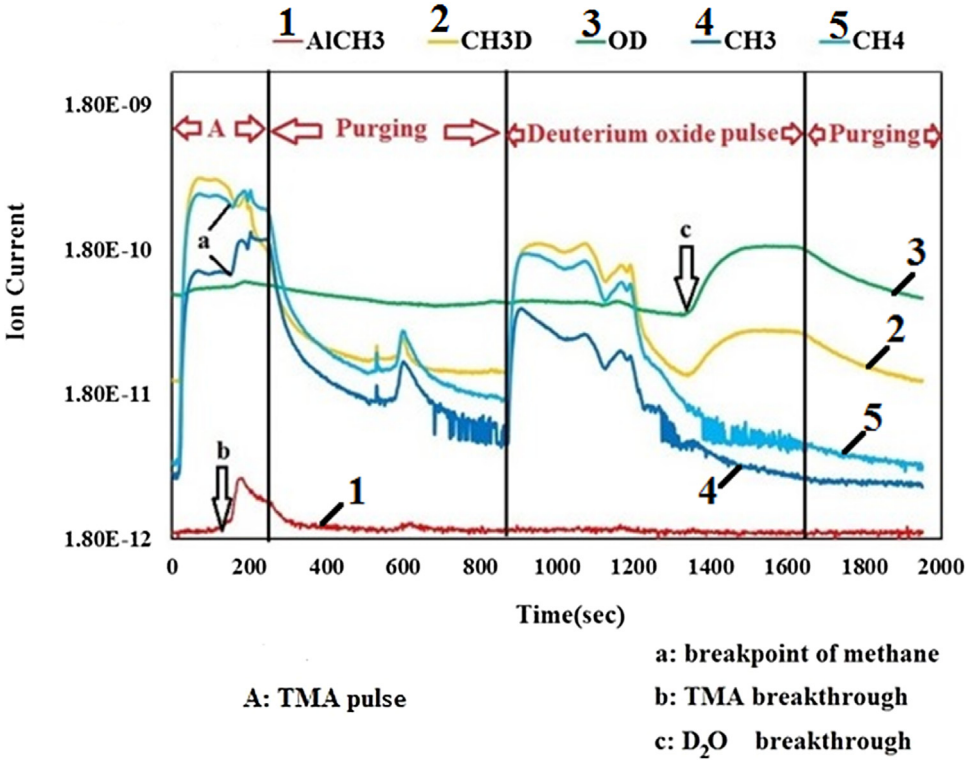

Fig. 4. Mass spectrum of TMA-D2O on TiO2 P25 during cycle 2.

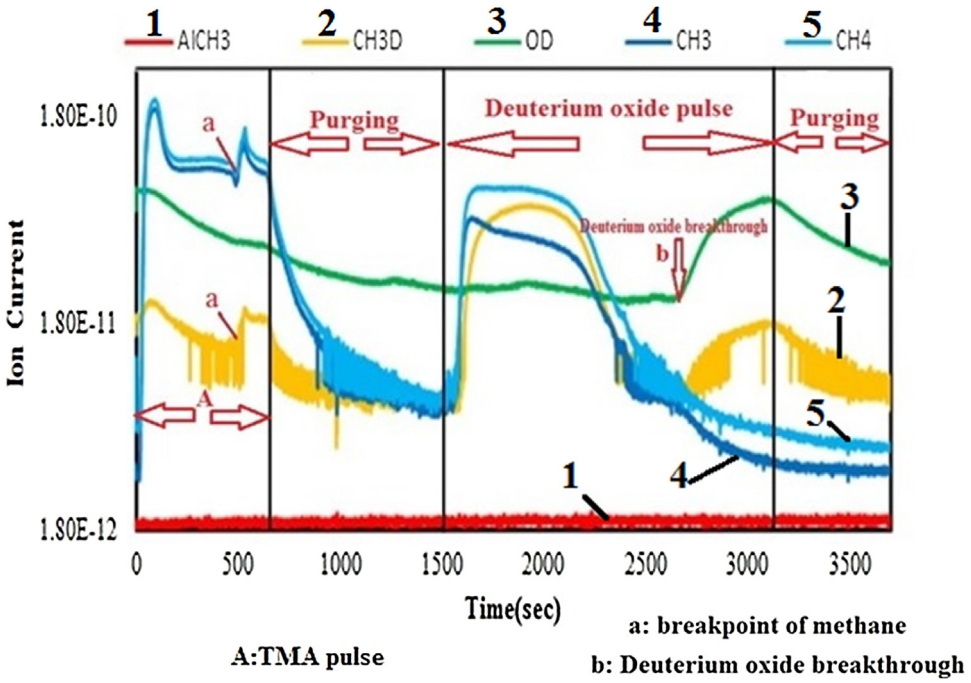

Fig. 5. Mass spectrum of TMA-D2O ALD on silica gel during cycle 1.

Table 1
Species detected by analysis of the residual gas during ALD of alumina on TiO_2 P25 using TMA-O_3.

ALD film	Reactant A	Reactant A fragments	Reactant B	Reactant B fragments	Product
Alumina	TMA	$Al(CH_3)_{3(m/z=72)}$ $Al(CH_3)_{2(m/z=57)}$ $Al(CH_3)_{(m/z=42)}$	Ozone	$O_{2(m/z=32)}$	$CH_{3(m/z=15)}$ $CH_{4(m/z=16)}$ $H_2O_{(m/z=18)}$ $CO_{2(m/z=44)}$

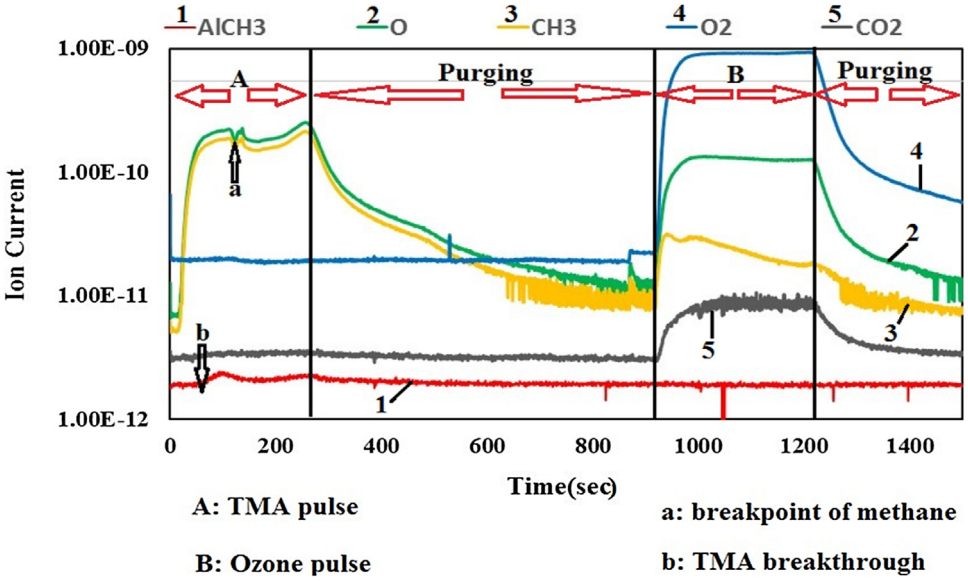

Fig. 6. Mass spectrum of TMA-Ozone ALD on TiO_2 P25.

The entire molecules and their fragments during exposure of TMA and ozone, derived through the ionization in the mass spectroscopy, are listed in Table 1.

Since the oxygen signal at m/z=16 interferes with the signal of methane, methane can be detected through the peak at 15 and the oxygen should be monitored by the peak at 32. As can be seen in Fig. 6, when TMA is fed to the reactor, the gas phase species from the first half of reaction (reaction of TMA with active sites) are very similar to the reaction products observed during the reaction (1). Chemisorption of TMA on the surface of titania nanoparticles leads to release of methane during dosing of TMA therefore methane is observed to increase linearly with time. Only after the reaction is nearly complete throughout the bed, the peak of generated methane begins to level off and the breakthrough of TMA is observed. Methane can be detected in Fig. 6 during exposure of both TMA and ozone. Carbon dioxide and its fragmentation product CO are released only during the ozone half reaction as can be seen in reaction (9).

During the second half of reaction (reaction (9)), ozone reacts with $AlCH_3$* species and methoxy ($AlOCH_3$*), formate (Al(OCHO)), carbonate (Al(OCOOH)) and hydroxyl (AlOH) groups are formed by insertion of an oxygen atoms into the Al—C and C—H bonds. Methoxy group is stable only at low temperature and formate species are formed by combining two methoxy groups with each other. This reaction is also the source of methane which was detected by mass spectrometry. Further oxidation of the formate group yields carbonate group and its decomposition releases CO and CO_2 species. In fact, formate and carbonate species release CH_4, CO and CO_2 to produce AlOH* species. Water is another byproduct during ozone pulse in TMA-ozone ALD process which is a very important species from the technological point of view [65].

Water is an important species whose presence should be investigated as a reaction byproduct during the ozone half reaction. Water can affect conformity of the film on nanoparticles, e.g., if water is formed during the ozone half reaction and the purging between TMA and ozone is insufficient, growth due to chemical vapor deposition type can lead to thickness non-uniformity [65]. Thus, existence of this byproduct was checked during the ozone half reaction as shown in Fig. 7. It can be seen in this figure that no water was detected by the mass spectrometer during ozone exposure. As reported by Rose et al. [65], detection of water depends on the reactive surface area and the ozone concentration. If these were high, detection of water as a byproduct of TMA/O_3 ALD would be possible. In fact, at high concentration of ozone, the surface consists of some chemisorbed active oxygen and —OH groups, leading to the release of water in the ozone pulse. In addition, intensity of the water signal increases in the high substrate surface area. Then, there would be few chemisorbed active oxygen on the surface of substrate at low concentration of ozone and existing H_2O is also consumed by producing —OH terminated surface [59].

More work should be done for investigating the formation of water at other temperatures. The same reaction products were suggested in the mechanism proposed by Goldstein et al. [59] who studied ALD of Al_2O_3 on ZrO_2 particles using sequential exposures of TMA and ozone. The data obtained in this work suggest that ALD in a fluidized bed reactor can be carried out in a manner that no precursor is wasted. The similar phenomenon was observed in the second cycle.

3.2. Quality of coating

3.2.1. Alumina coating on titania nanoparticles with TMA-water/deuterium oxide

Fig. 8a–c show TEM images of titania particles coated by alumina with TMA-water after 4, 7 and 10 ALD cycles. The film thickness was measured at a number of locations (20 locations in 4 cycles, 15 locations in 7 cycles and 15 locations in 10 cycles) to determine the conformity of Al_2O_3 coating on TiO_2 nanoparticles. The deposited amorphous alumina layer can be easily distinguished from the crystalline titania substrate in these figures. The average GPC was measured from TEM images as 0.17 nm for 4 and 7 cycles, and 0.14 nm for 10 cycles. The average GPC for these three tests is about 0.16 nm which is close to the previously reported value [19]. The film thickness calculated using the mass fraction of alumina from the equation suggested by Valdesueiro et al. [19] and also measured by INAA support the value obtained from the TEM images. Density of alumina for evaluating the thickness by equation of Valdesueiro et al. [19] was considered to be 3000 kg/m^3 which is typical for Al_2O_3 ALD at 177 °C [19]. The average GPC was estimated to be ~0.17 nm based on this method which indicates a linear correlation between the number of cycles and the film thickness from INAA. Mass fraction of aluminum measured by INAA analyses as well as the volume of alumina film and the film thickness obtained by INAA measurements for alumina ALD using TMA-Water on tita-

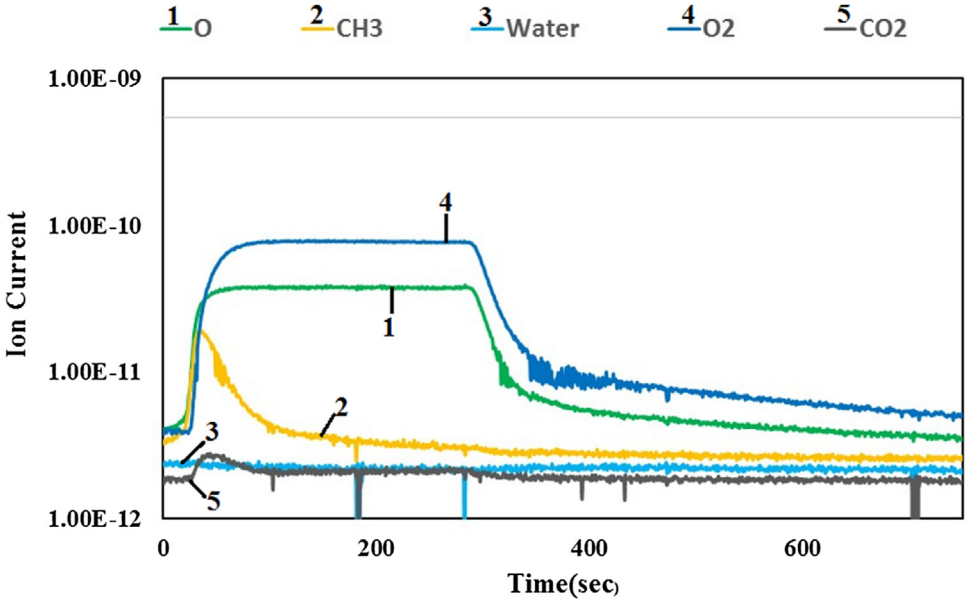

Fig. 7. Mass spectrum of TMA-Ozone ALD on TiO2 P25 during ozone half reaction.

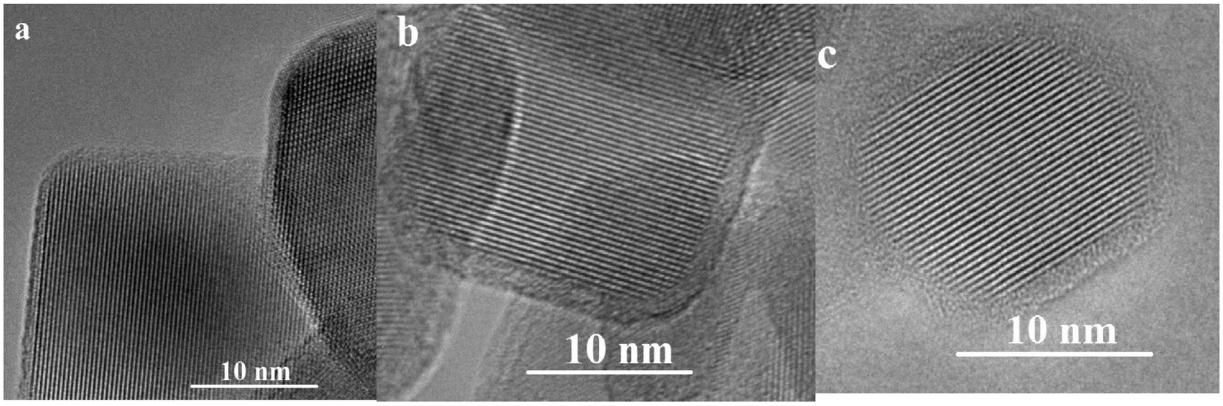

Fig. 8. TEM images of the alumina film deposited on titania nanoparticles using TMA-water after (a) 4 cycles (b) 7 cycles (c) 10 cycles.

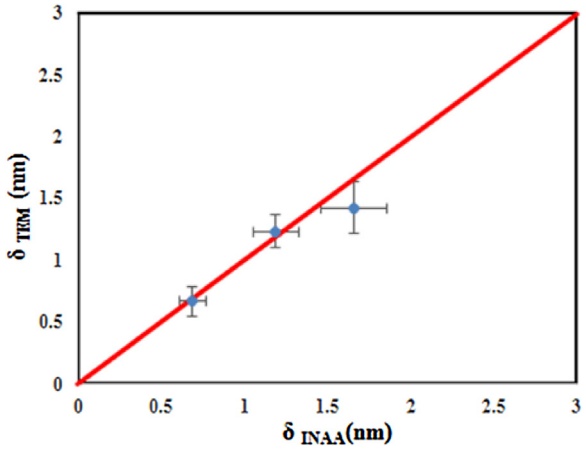

Fig. 9. Comparison of the alumina film thickness measured by TEM and INAA after 4, 7 and 10 cycles of alumina ALD using TMA-water on TiO2 P25.

nia nanoparticles are listed in Table S3 (Supplementary Information S3).

Comparison of the film thickness measured by TEM and INAA is shown in Fig. 9. As can be seen in this figure, the thickness of alumina film from TEM images are in reasonable agreement with those measured by INAA. The error bars in Fig. 9 indicates the error in the measurements obtained from the propagation of the uncertainty and calculated from the formula suggested by Valdesueiro et al. [19].

EDX analysis was conducted to determine which elements are present on the surface of the substrate. In Fig. 10 elemental maps of O, Ti and Al are shown of part of a coated particle form the 10-cycle experiment on the support foil as well as the ADF image of the scanned area. The edge of the particle shows excess of Al compared to the interior of the particle. This is even more evident when more particles are mapped as in Fig. S8 (Supplementary Information) and is consistent with a TiO_2 core/Al shell structure. Note that the width of the edge with excess Al content is from a projected structure. Hence, an inclined edge, i.e. partly not parallel to the electron beam, will exaggerate the width. In addition, X-rays and secondary electrons generated by the electron beam positioned in the core will generate some Al X-rays, again exaggerating the shell width compared to the values measured in the TEM images like Fig. 8. In Fig. 10 a comparison is made between the EDX spectra for two locations on the particle: the edge and the bulk as indicated in the ADF of Fig. 10. The Cu L-lines are from secondary electrons (generated by the electron beam) hitting the copper grid that holds

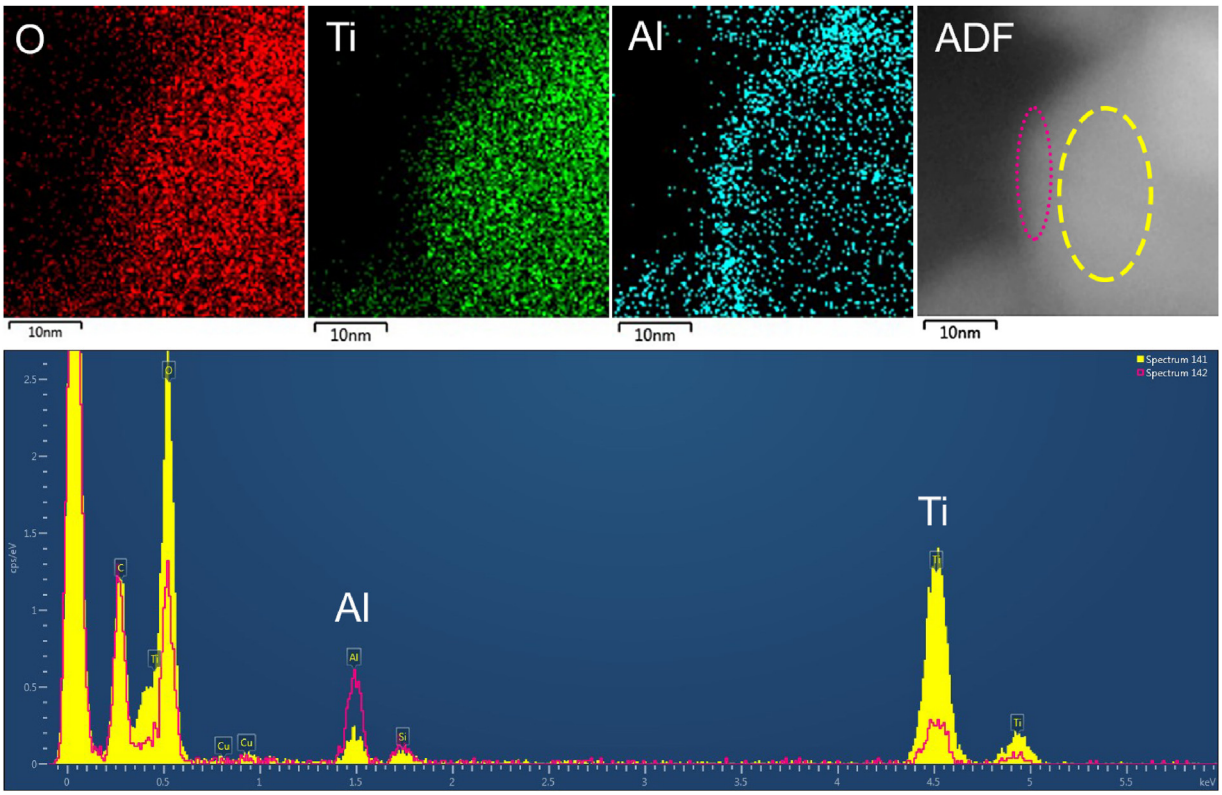

Fig. 10. EDX spectra and EDX mapping from a coated particle after 10 cycles of alumina ALD using TMA-water. The solid yellow spectrum and the red outlined spectrum are from the interior and the edge of the particle as indicated by the dashed and dotted areas respectively in the ADF. (For interpretation of the references to colour in this figure legend, the reader is referred to the web version of this article.)

the carbon support foil that the particles were placed on it. The Si lines are caused by an impurity on the support foil always present on the grids purchased from Quantifoil. As can be seen, the Al line in the spectrum from the edge of the particle (red line) is higher than the Al line in the spectrum form bulk of the particle (solid yellow). This confirms that the Al coat is formed on the surface of the particle. For the same reason, the intensity of Ti line in the bulk of particle is larger than that from the edge. The Al peak in the bulk spectrum is related to the coating on surfaces perpendicular to the electron beam.

Similar results were obtained when using deuterium oxide instead of water. TEM images of the Al_2O_3 coated titania nanoparticles with TMA-deuterium oxide are presented in Fig. S4 (a)-(c) (Supplementary Information S3) which provide visual confirmation of presence of Al_2O_3 film on the particle surface. The GPC at a number of points and particles (33 location in 4 cycles, 37 location in 7 cycles and 20 location in 10 cycles) were measured and compared with those measured by mass fraction of aluminum from INAA to support the results obtained from the TEM images which can be seen in Table S4 (Supplementary Information S3). Comparison of the film thickness measured by TEM images and INAA is shown in Fig. S5 (Supplementary Information S3) which shows a good agreement between the thicknesses determined by these two methods. Also, mass fraction of aluminum measured by INAA, volume of film and GPC of this measurement for 4, 7 and 10 cycles are listed in Table S4 (Supplementary Information S3).

To determine the elemental composition at the surface of the substrate, EDS analysis was carried out. Fig. 11 shows the Ti and Al presence in the same elemental map, next to the ADF image of a group of particles. In the lower right corner some particles overlap leading to an increase of intensity for Ti. Fig. S8 (Supplementary Information S3) shows the Al, Ti and O maps separately.

Fig. S6 (Supplementary Information S3) compares the EDX spectra at two locations (edge and bulk) of a particle taken from the 10 cycle experiment. Similar results were obtained when using deuterium oxide instead of water. Same results can be seen for HRTEM image shown in Fig. S7 (Supplementary Information S3) which indicates atomic percent of Al increases from 3 on the bulk to 26 on the edge of particle.

To indicate the importance of purging time in conformity of coating and GPC, a set of experiments were performed at excess dosing time of TMA and deuterium oxide (10 times the ideal dosing time). Figs. S9 (a)–(c) (Supplementary Information S3) show TEM images of titania particles after alumina coating with TMA-deuterium oxide for 4, 7 and 10 ALD cycles, respectively. The film thickness at a number of particles (17 location in 4 cycles, 33 location in 7 cycles and 9 location in 10 cycles) was measured to determine the conformity of Al_2O_3 coating on TiO_2 nanoparticles. Mass fraction of aluminum measured by INAA, volume of alumina film and film thickness calculated from the INAA measurements for this set of experiments are given in Table S5 (Supplementary Information S3). The film thickness in this case is slightly more than those conducted when using optimum dosing time and also the uniformity in this case is less than the previous case. However, the average GPC in this set of experiments is about 0.16 nm which is close to that reported by Valdseruio et al. [19] for alumina coating. The GPC determined from TEM images and INAA are compared in Fig. S10 (Supplementary Information S3). As can be seen in this figure, there is a discrepancy between the GPC of alumina film from TEM images and those from INAA. This can be attributed to using different oxidizers which may lead to a different alumina density than the assumed value of 3000 kg/m^3 which affect the calculated film thickness by INAA. Fig. S11 (Supplementary Information S3) shows the EDX elemental mapping and a line scan across the edges

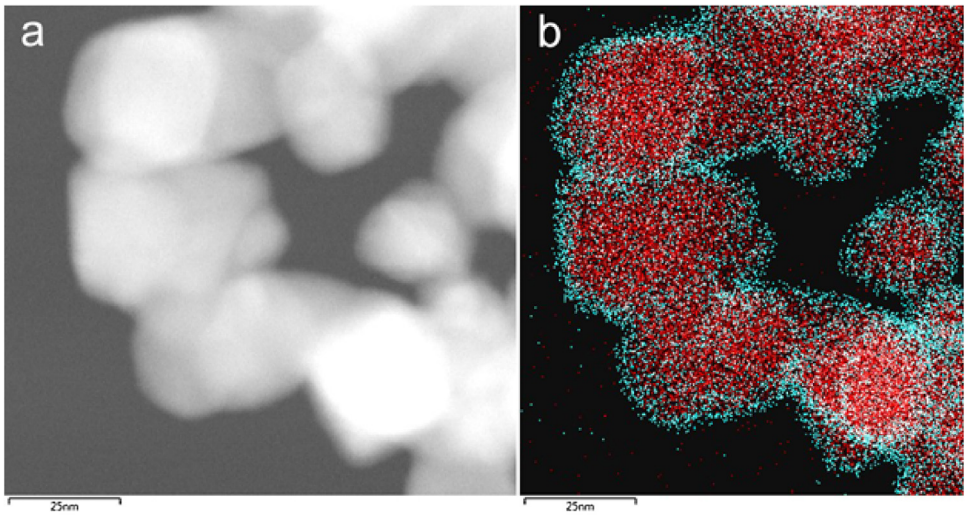

Fig. 11. a) ADF image of a group of particles (10 cycles of alumina ALD using TMA- deuterium oxide on TiO2 P25) suspended above a hole in the supporting carbon foil. b) Overlapping elemental maps from STEM EDX for Al (blue at the edge) and Ti (red in the interior) next to the ADF image of the mapped area on the left. (For interpretation of the references to colour in this figure legend, the reader is referred to the web version of this article.)

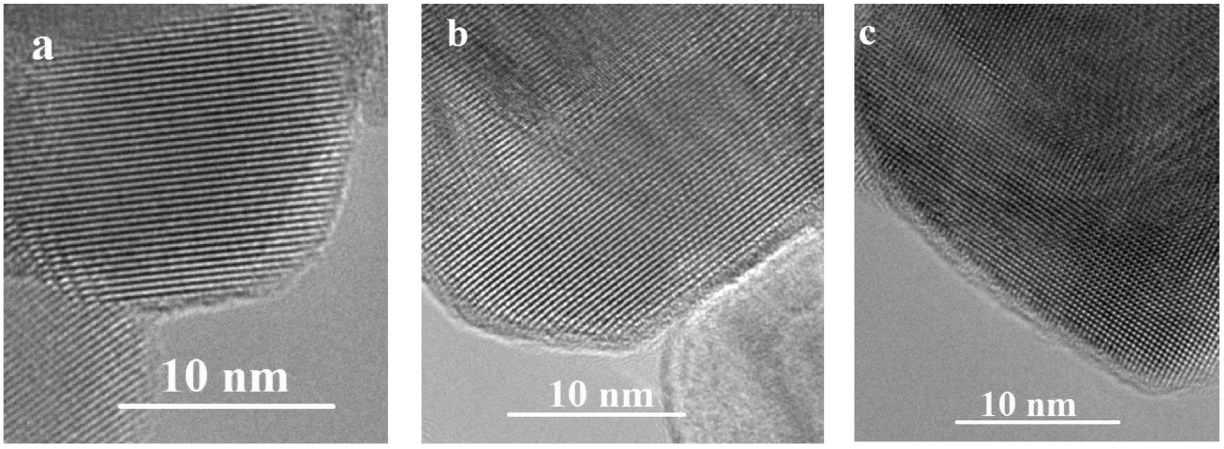

Fig. 12. TEM images of the alumina layer deposited using TMA-ozone on titania nanoparticles after (a) 4 cycles (b) 7 cycles (c) 10 cycles.

of particles for alumina ALD with excess TMA and 7 min purging time. Similar results to Fig. 10 can be seen in this figure.

3.2.2. *Alumina coating with TMA-ozone*

Figs. 12(a)–(c) show the alumina layer deposited on the surfaces of primary titania nanoparticles using TMA-ozone. The amorphous alumina film can be easily distinguished from the highly crystalline titania substrate. The thickness of the alumina film at a number of locations and particles (10 locations in 4 cycles, 16 locations in 7 cycles and 22 locations in 10 cycles) was measured and compared with those from INAA, as can be seen in Fig. 13. This figure demonstrates that there is a reasonable agreement between these two measurements. Aluminum mass fractions measured by INAA as well as the GPC measured by INAA are listed in Table S6 (Supplementary Information S3). The GPC calculated from mass fraction of aluminum (INAA) results in a GPC of about 0.12 nm which is slightly greater than that observed in TEM images which is about 0.11 nm. This GPC is less than the that of alumina film when using water and deuterium oxide as oxidizer.

Fig. 14. shows EDX line and mapping of the surface of particles after 10 cycles of alumina ALD using TMA-ozone. The image with rectangle shows the area where the elemental maps were taken. Formation of alumina layer can be easily seen in this map (blue shell of alumina). Also, line scan across the alumina layer can be seen in this figure. The line scan shows the thickness is ~1.2 nm which is close to the value obtained from TEM images which can

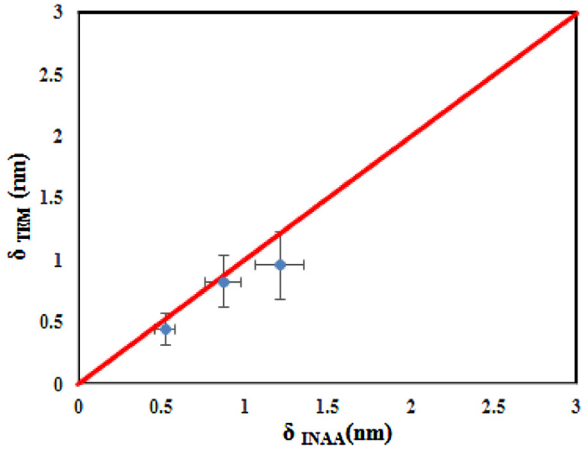

Fig. 13. Comparison of the film thickness measured by TEM images and INAA analysis after 4, 7 and 10 cycles of alumina ALD using TMA-ozone on TiO2 P25.

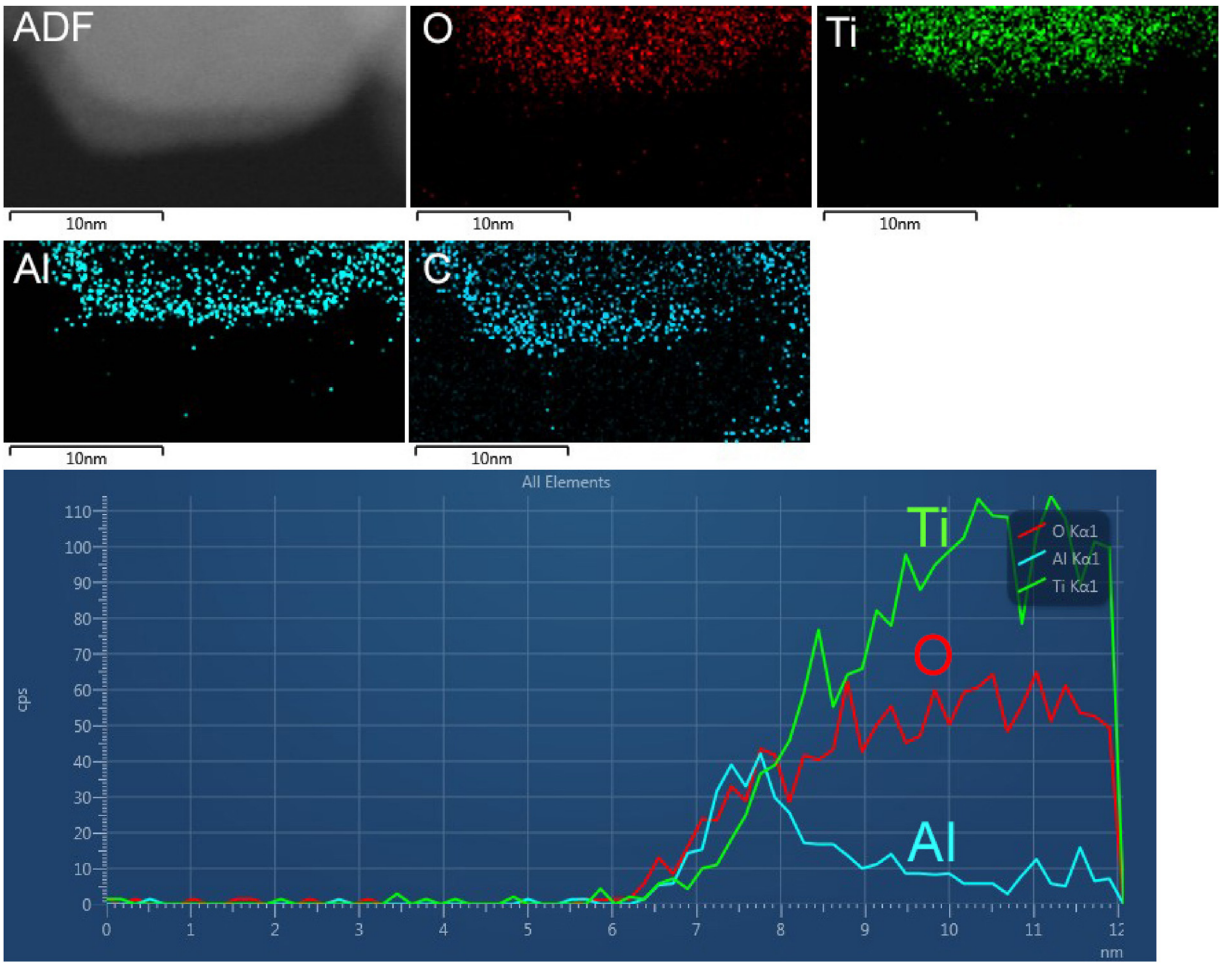

Fig. 14. ADF image and EDX maps from part of a titania particle suspended above a hole in the support foil, after 10 cycles of alumina ALD using TMA-ozone.

be seen in Fig. 13. Note carbon contamination at the edge of the particle is present caused by the electron beam during scanning.

Comparison of measured film thickness from TEM images and those from INAA for different oxidizers are presented in Fig. 15 (a) and (b). It can be seen in these figures that the film grows linearly. Thickness of the alumina layer formed by ALD of TMA-ozone is less than that of other oxidizers. Alumina ALD with TMA-water is based on acid-base reactions in which H^+ from OH group combines with $(CH_3)^-$ to form CH_4, while Al and O bond together to form Al_2O_3 product on the surface (reaction (3)). Consequently, the growth rate is higher as more H^+ becomes available. In fact, as shown by Elliot et al. [71,72], the GPC scales linearly with the amount of H^+ (i.e., OH groups). It should be noted that the different co-reagents may lead to different densities of films which means that the thickness change per cycle may not exactly reflect the mass change per cycle.

As a co-reagent, water can deliver as much H^+ as needed, saturating the surface with OH groups and providing the maximum surface coverage of H^+ at a given process temperature. This obviously leads to a greater GPC for water when compared to ozone as the oxidizing agent. Although no mechanism has been proposed for the reaction yet, it can be said that H_2O adsorbs onto under-coordinated Al atoms and dissociates, donating H^+ to nearby O or CH_3 groups which the latter is desorbed as CH_4. Water continues to adsorb onto alumina and dissociate until the saturating coverage on alumina at the process temperature is reached. This results in a higher coverage of surface by OH, leading to a greater GPC. The higher GPC for alumina ALD using water as the co-reagent than ozone as oxidizer has been reported in literature [66,71]. Ozone oxidizes CH_3 groups on the surface, producing various volatile products (CO_2, CO, H_2O, etc.) plus an OH group on the surface (reaction 9). As a simple rule, each CH_3 group oxidizes to one OH group. The amount of H^+ (i.e., OH groups) is, therefore, limited by the amount of CH_3 saturating the surface in the previous pulse. CH_3 is quite a bulky ligand and steric hindrance caused by CH_3 ligands can shield parts of the surface from being accessible to the precursor. This means that the OH coverage is low and consequently, the GPC of alumina in case of ozone as oxidizer is less than that of water.

Another point in Fig. 15(b) is that in the case of using excess precursor (10 times the ideal dosing time), the film thickness is greater than in other cases. This can be attributed to the issue that the purging time in case of excess dosing has not been enough to evacuate all unreacted molecules. This purging time was set to about 13 times the residence time of the gas in the reactor [19]. Due to insufficient purging time in this set of experiments, unreacted molecules were accumulated on the surface of the particles, resulting in occurrence of slight parasitic chemical vapor deposition (CVD) reaction and a greater GPC. This unwanted reaction can result in an alumina layer with different density than the assumed 3000 kg/m^3 which affects calculation of the film thickness from mass fraction of aluminum measured by INAA. However, the film thickness and GPC for this case are still in the range of ALD and it seems that the unwanted reactions were not too problematic. These results show the advantage of using mass spectrometry to determine exact dosing time of the precursor to avoid undesired reactions during the deposition process.

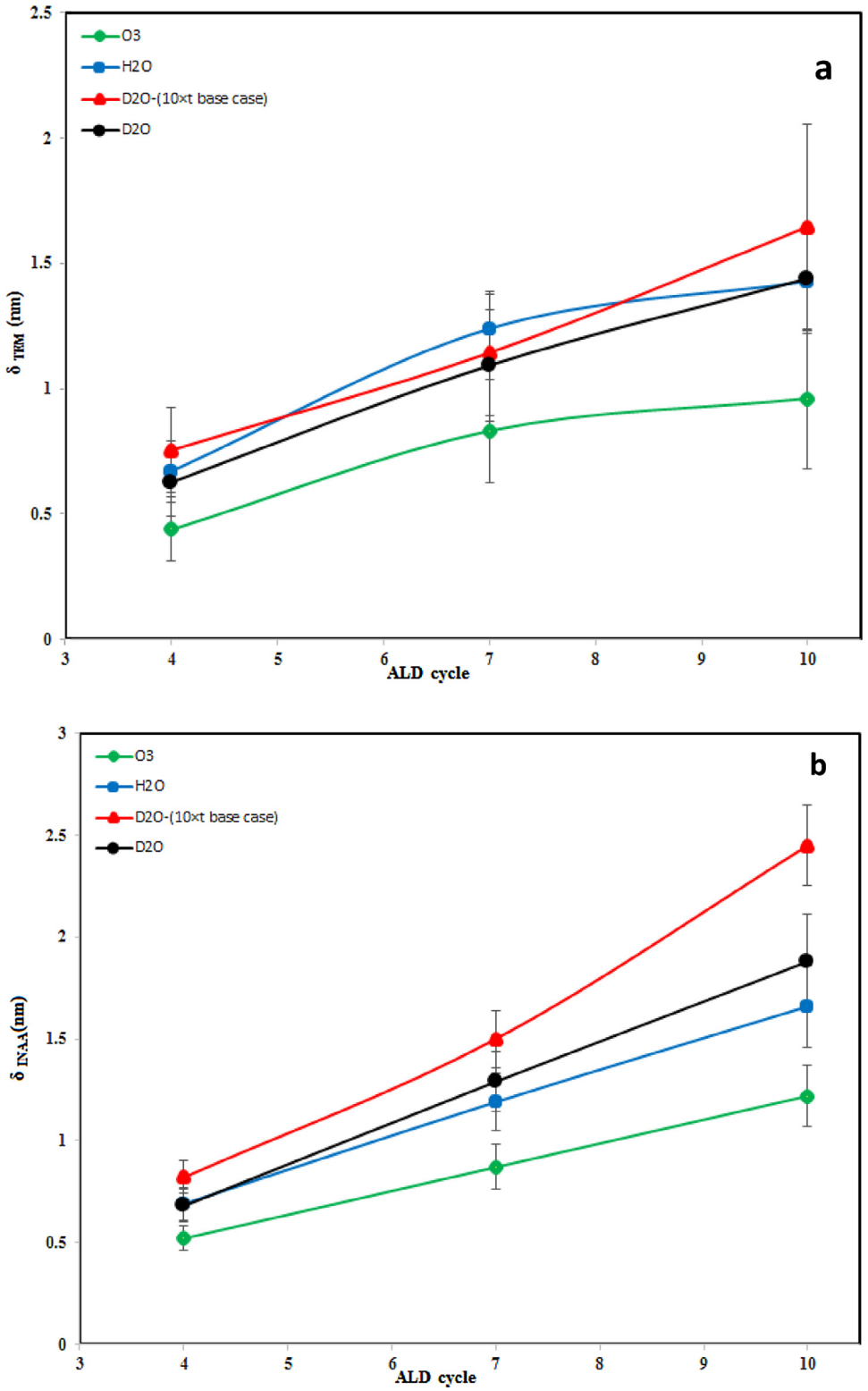

Fig. 15. Alumina film thickness on TiO_2 P25 against number of cycles for different oxidizers measured from a) TEM images b) INAA.

When using deuterium oxide or water, the coated particles exhibit a blue color. This can be attributed to reduction of Ti^{4+} to Ti^{3+} cations because Ti^{3+} ions are origin of blue coloration. When using ozone in the subsequent pulse, oxidation would remove the blue color, whereas H_2O and D_2O are not strong enough oxidizing agents to do this and the blue color persists. This change in the color of particles to blue and green was also reported by King et al. [73].

3.2.3. BET measurements

The surface area of five particle samples, including bare titania and coated after 10 cycles using different oxidizers, were measured with the BET method. The coated samples showed similar adsorption and desorption isotherms as shown in Fig. S12 (Supplementary Information S4). Since there is no significant hysteresis in the isotherm of coated samples, it can be concluded that either

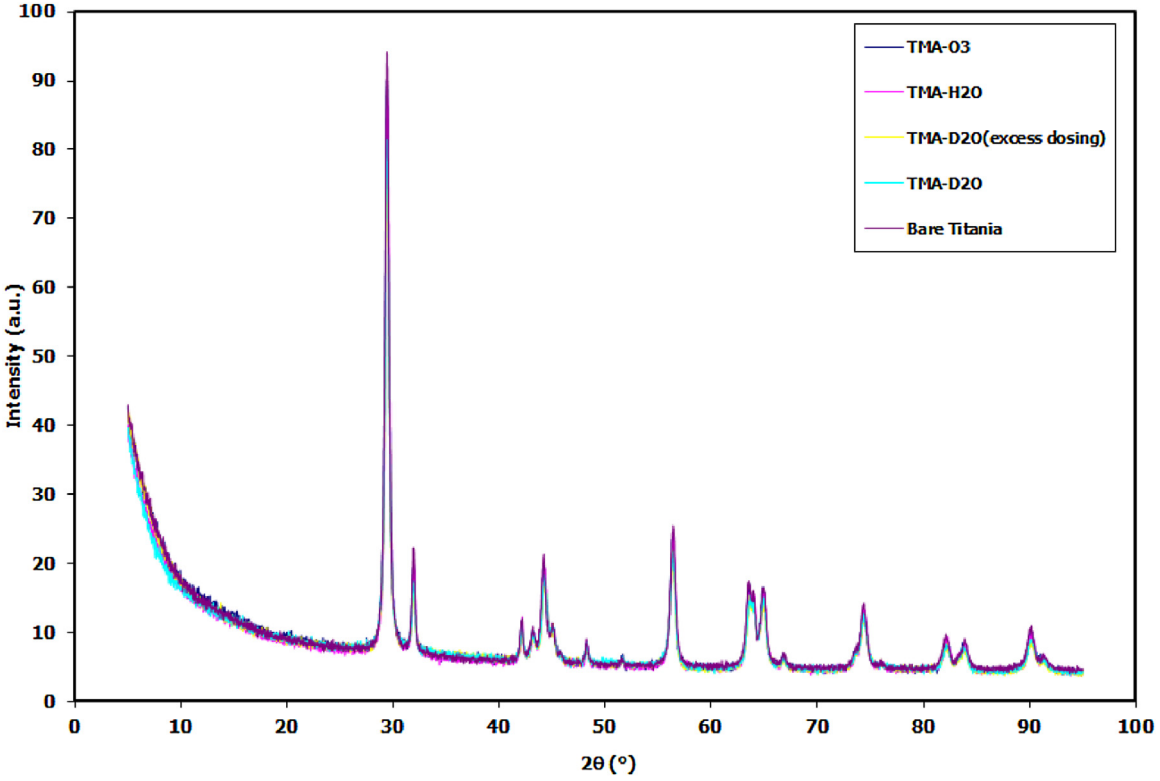

Fig. 16. XRD spectra of uncoated and coated titania particles after 10 cycles of alumina ALD using different oxidizers.

there are no pores in the films or the pores have a small volume. It should be noted that no pores were visible in the TEM images. Similar results were reported by Valdesueiro et al. [19].

Although the surface area decreases during the coating process, this variation cannot be attributed to agglomeration of nanoparticles. If agglomerates are coated as a whole, the equivalent particle diameter of the coated material would be close to the agglomerate size (in order of micro meters) and a drastic decrease in the specific surface area of the powder should be observed. The results obtained from high resolution TEM, STEM and EDX mapping (e.g., Figures (8) and (S8) (Supplementary Information S3)) show that the coating was applied on the primary particles rather than agglomerates. This can be also confirmed by evaluating the size of particles based on the BET measurement. The equivalent particle diameter (d_{BET}) can be obtained from the specific surface area [74]:

$$d_{BET} = \frac{6000}{\rho S_{BET}} \quad (10)$$

Measured surface area and particles diameters of coated particles using BET are presented in Table S7 (Supplementary Information S3). According to this table, the surface area of coated nanoparticles has decreased compared to the uncoated samples and the equivalent particle diameter has increased slightly after coating. Decrease of the specific surface area of particles after coating can be attributed to increase in the size of titania nanoparticles due to alumina coating and also decreasing of the core-shell particle density.

3.2.4. XRD analyses

Fig. 16 shows XRD spectra of bare titania and the samples coated after 10 cycles using different oxidizers. These spectra are all the same which means that there is no change in the crystalline structure of the base material after formation of Al_2O_3 layer. Similarity of XRD spectra of coated and uncoated materials was expected since the alumina coatings are amorphous. Also, TEM images (e.g., Figs. 8 and 12) show that amorphous alumina layer has been deposited on crystalline titania nanoparticles. Previous studies also confirm the amorphous nature of alumina films deposited by ALD [22].

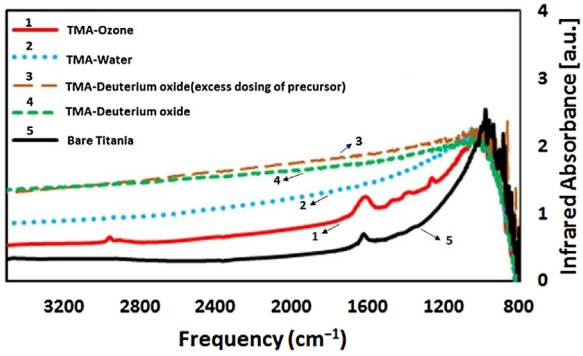

Fig. 17. Fourier transform infrared spectra of uncoated and coated titania nanoparticles after 10 cycles.

3.2.5. FTIR analyses

FTIR spectra of coated and uncoated titania particles are shown in Fig. 17. The vibrational modes of amorphous alumina film and Ti–O bond are located at frequency range of 850–1050 cm^{-1} [11] and 800–980 cm^{-1} [75], respectively. Intensity of the peak related to Ti–O bond is attenuated for the coated sample with deuterium oxide, water and ozone when compared to the bare titania. The intensity is less when ozone was used as the oxidizer. This can be attributed to the fact that a thicker film leads to more attenuation in the intensity of the peak related to Ti–O bond. Fig. 17 also demonstrates that there is a vibrational mode around 1500 cm^{-1} for the sample coated with TMA-ozone. This new absorbance feature is a characteristic of formate and carbonate groups on the Al_2O_3 layer,

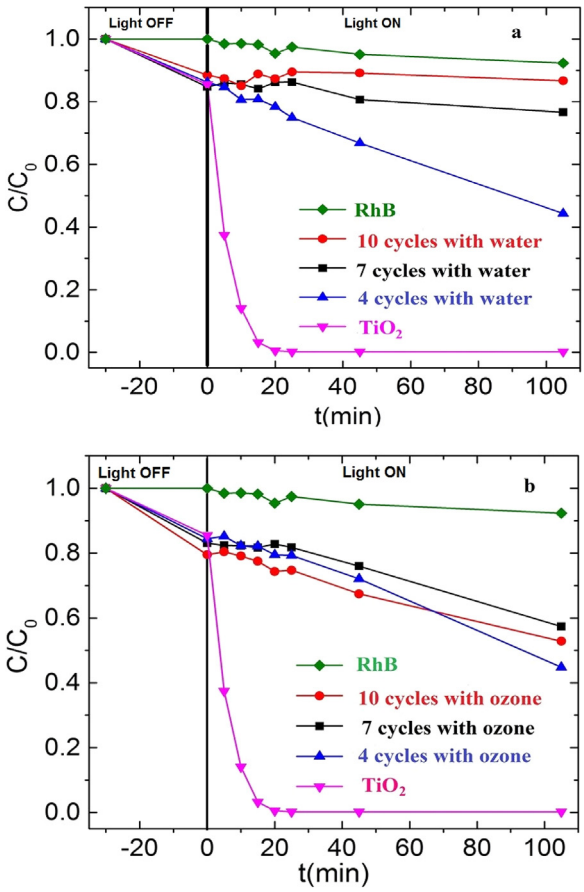

Fig. 18. RhB concentration in photocatalytic tests as a function of UV irradiation time for alumina ALD film with TMA and different oxidizer at different cycles a) water b) ozone.

formed according to reaction (9). The absorption features located at 1388 and 1597 cm^{-1} correspond to O—C—O modes of vibration of formate species. Presence of formate groups on the surface was confirmed by Goldstein et al. [59] after exposure of ozone on the zirconia substrate. The peak around 1650 cm^{-1} shows that water is adsorbed on the sample. This peak disappears if the sample is heated or dry air is used.

3.3. *Passivation effect of alumina ALD films*

Titania is not only widely used as the white pigment in industrial applications, but is also a well-known UV-activated oxidation catalyst which degrades the polymer surrounding the pigment. To ensure that the photo catalytic activity of the pigment is decreased, formation of free radicals should be prevented. This can be achieved by preventing photo-generated electrons and holes from reaching the titania particle surface. Establishing an ultrathin film coating on titania particle is a suitable approach to decrease the photoactivity of titania nanoparticles. Coating with 3–5 wt% alumina is widely used in industry for preventing photocatalytic activity of these particles.

Fig. 18(a) and (b) demonstrate the photocatalytic activity of alumina-coated titania nanoparticles, measured by degradation of Rhodamine B under ultraviolet irradiation. Photocatalytic activities of titania nanoparticles having different thicknesses of deposited alumina film using TMA and various oxygen sources are shown in these figures. The self-degradation of RhB was about 7%. The relative concentration of RhB in the solution decreases exponentially with the UV irradiation time and RhB can be degraded completely by TiO_2 after about 20 min. In contrast, coated TiO_2 particles showed mitigated photoactivity with increasing the coating thickness. For example, Fig. 18(a) shows that in the presence of particles coated with TMA-water, the relative concentration reached 0.45, 0.78 and 0.90 for 4, 7 and 10 ALD cycles, respectively, after 100 min. UV irradiation. Similar results can be reached when using TMA-deuterium oxide for ALD, as shown in Fig. S13 (Supplementary Information S4). Fig. 18 (b) demonstrates that the deactivation is less when using ozone as the oxidizing agent. The reason is the lower film thickness when ozone is used (see Fig. 15a) which results in lower deactivation of the particles when compared with water as co-reactant. As can be seen in Fig. 18b, the photocatalytic activity of nanoparticle hardly changes with the number of ALD cycles. Since Al_2O_3 has a high band gap, if the Al_2O_3 layer is thick enough, electrons and holes in TiO_2 cannot pass through the alumina film to reach the surface of particle, and the photocatalytic activity is suppressed. The alumina thickness in the case of 7 and 10 cycles ALD using TMA-O_3 is less than 1 nm which is not thick enough to completely block the transfer of electrons and holes.

4. Conclusions

Aluminum oxide film was deposited on titania nanoparticles at 180 °C and 1 bar in an ALD fluidized bed reactor. Real time analysis of effluent gases from the reactor during each reaction cycle was conducted using an online mass spectrometer. Optimum dosing time of precursors was determined based on breakthrough of precursors in the mass spectrum. Different oxygen sources (water, ozone and deuterium oxide), in combination with TMA, were utilized to check which one provides the highest alumina GPC. Using either water or deuterium oxide as the oxygen source resulted in formation of a thicker alumina film on titania particles compared to ozone. Breakthrough of the TMA, which takes place nearly at the time of breakpoint of the methane signal, shows saturation of substrate surface with TMA. Similar to water breakthrough, the D_2O breakthrough does not take place at the maximum of the product signal (here, CH_3D) and does not increase until the CH_3D signal has considerably dropped. In the ozone half reaction, ozone oxidizes CH_3 group on the surface, producing various volatile products (CO_2, CO, CH_4, etc.) plus an OH group on the surface of the substrate. Average GPC measured by TEM was about 0.16 nm, 0.15 nm and 0.11 nm, respectively, in the ALD of TMA using water, deuterium oxide and ozone as the oxygen source. The average GPC measured by INAA was close to those measured by TEM. Formation of alumina film was confirmed using results obtained by EDX mapping and line for area of particles, XRD and FTIR. Results obtained by BET showed that the alumina film was formed on individual primary titania nanoparticles, rather than on agglomerates. FTIR also showed presence of formate groups on the surface of coated particles in the case of ozone exposure. Coated TiO_2 particles showed mitigated photoactivity with increasing the coating thickness. For example, for particles coated with TMA-water, the relative concentration reached 0.45, 0.78 and 0.90 for 4, 7 and 10 ALD cycles, respectively, after 100 min of UV radiation

Acknowledgment

The authors would like to thank Dr. David Valseruio, Dr. Simon Elliot, Fabio Grillo, Aris Goulas for their helps and valuable comments during this work.

Appendix A. Supplementary data

Supplementary data associated with this article can be found, in the online version, at http://dx.doi.org/10.1016/j.apsusc.2017.07.168.

References

[1] D.M. King, X. Liang, A.W. Weimer, Functionalization of fine particles using atomic and molecular layer deposition, Powder Technol. 221 (2012) 13–25.
[2] X. Liang, G.-D. Zhan, D.M. King, J.A. McCormick, J. Zhang, S.M. George, A.W. Weimer, Alumina atomic layer deposition nanocoatings on primary diamond particles using a fluidized bed reactor, Diamond Relat. Mater. 17 (2008) 185–189.
[3] S. Salameh, J. Gómez-Hernández, A. Goulas, H. Van Bui, J.R. van Ommen, Advances in scalable gas-phase manufacturing and processing of nanostructured solids: A review, Particuology 30 (2017) 15–39.
[4] C.L. Duan, Z. Deng, K. Cao, H.F. Yin, B. Shan, R. Chen, Surface passivation of Fe_3O_4 nanoparticles with Al_2O_3 via atomic layer deposition in a rotating fluidized bed reactor, J. Vacuum Sci. Technol. A 34 (2016) 04C103.
[5] D.M. King, X. Liang, B.B. Burton, M.K. Akhtar, A.W. Weimer, Passivation of pigment-grade TiO_2 particles by nanothick atomic layer deposited SiO_2 films, Nanotechnology 19 (2008) 255604.
[6] L.F. Hakim, J. Blackson, A.W. Weimer, Modification of interparticle forces for nanoparticles using atomic layer deposition, Chem. Eng. Sci. 62 (2007) 6199–6211.
[7] J. Guo, S. Yuan, Y. Yu, J.R. van Ommen, H. Van Bui, B. Liang, Room-temperature pulsed CVD-grown SiO_2 protective layer on TiO_2 particles for photocatalytic activity suppression, RSC Adv. 7 (2017) 4547–4554.
[8] D.M. King, X. Liang, Y. Zhou, C.S. Carney, L.F. Hakim, P. Li, A.W. Weimer, Atomic layer deposition of TiO 2 films on particles in a fluidized bed reactor, Powder Technol. 183 (2008) 356–363.
[9] D.M. King, J.A. Spencer, X. Liang, L.F. Hakim, A.W. Weimer, Atomic layer deposition on particles using a fluidized bed reactor with in situ mass spectrometry, Surf. Coat. Technol. 201 (2007) 9163–9171.
[10] X. Liang, K.S. Barrett, Y.-B. Jiang, A.W. Weimer, Rapid silica atomic layer deposition on large quantities of cohesive nanoparticles, ACS Appl. Mater. Interfaces 2 (2010) 2248–2253.
[11] L.F. Hakim, J.A. McCormick, G.D. Zhan, A.W. Weimer, P. Li, S.M. George, Surface modification of titania nanoparticles using ultrathin ceramic films, J. Am. Ceram. Soc. 89 (2006) 3070–3075.
[12] L.F. Hakim, J. Blackson, S.M. George, A.W. Weimer, Nanocoating individual silica nanoparticles by atomic layer deposition in a fluidized bed reactor, Chem. Vap. Deposition 11 (2005) 420–425.
[13] X. Liang, A.W. Weimer, An overview of highly porous oxide films with tunable thickness prepared by molecular layer deposition, Curr. Opin. Solid State Mater. Sci. 19 (2015) 115–125.
[14] H.V. Van Bui, F. Grillo, R. Helmer, A. Goulas, J.R. van Ommen, Controlled growth of palladium nanoparticles on graphene nanoplatelets via scalable atmospheric pressure atomic layer deposition, J. Phys. Chem. C 120 (2016) 8832–8840.
[15] A. Lubers, A. Drake, D. Ludlow, A. Weimer, Electrochemical hydrogen pumping using a platinum catalyst made in a fluidized bed via atomic layer deposition, Powder Technol. 296 (2016) 72–78.
[16] A. Goulas, J.R. van Ommen, Scalable production of nanostructured particles using atomic layer deposition, KONA Powder Particle J. 31 (2014) 234–246.
[17] F. Grillo, M.T. Kreutzer, J.R. van Ommen, Modeling the precursor utilization in atomic layer deposition on nanostructured materials in fluidized bed reactors, Chem. Eng. J. 268 (2015) 384–398.
[18] R.L. Puurunen, Surface chemistry of atomic layer deposition: a case study for the trimethylaluminum/water process, J. Appl. Phys. 97 (2005) 121301.
[19] D. Valdesueiro, G.M. Meesters, M.T. Kreutzer, J.R. van Ommen, Gas-Phase deposition of ultrathin aluminium oxide films on nanoparticles at ambient conditions, Materials 8 (2015) 1249–1263.
[20] J.R. van Ommen, D. Kooijman, M. de Niet, M. Talebi, A. Goulas, Continuous production of nanostructured particles using spatial atomic layer deposition, J. Vacuum Sci. Technol. A 33 (2015) 021513.
[21] C. Soria-Hoyo, J. Valverde, J. van Ommen, P. Sánchez-Jiménez, L.A. Pérez-Maqueda, M. Sayagués, Synthesis of a nanosilica supported CO_2 sorbent in a fluidized bed reactor, Appl. Surf. Sci. 328 (2015) 548–553.
[22] R. Beetstra, U. Lafont, J. Nijenhuis, E.M. Kelder, J.R. van Ommen, Atmospheric pressure process for coating particles using atomic layer deposition, Chem. Vap. Deposition 15 (2009) 227–233.
[23] S.M. George, Atomic layer deposition: an overview, Chem. Rev. 110 (2010) 111–131.
[24] S.M. George, B. Yoon, A.A. Dameron, Surface chemistry for molecular layer deposition of organic and hybrid organic- inorganic polymers, Acc. Chem. Res. 42 (2009) 498–508.
[25] A. Goulas, J.R. van Ommen, Atomic layer deposition of platinum clusters on titania nanoparticles at atmospheric pressure, J. Mater. Chem. A 1 (2013) 4647–4650.
[26] L.F. Hakim, S.M. George, A.W. Weimer, Conformal nanocoating of zirconia nanoparticles by atomic layer deposition in a fluidized bed reactor, Nanotechnology 16 (2005) S375.
[27] X. Liang, L.F. Hakim, G.D. Zhan, J.A. McCormick, S.M. George, A.W. Weimer, J.A. Spencer, K.J. Buechler, J. Blackson, C.J. Wood, Novel processing to produce polymer/ceramic nanocomposites by atomic layer deposition, J. Am. Ceram. Soc. 90 (2007) 57–63.
[28] J.R. Van Ommen, Apparatus and process for atomic or molecular layer deposition onto particles during pneumatic transport, in, Google Patents, 2010.
[29] Y. Zhou, D.M. King, X. Liang, J. Li, A.W. Weimer, Optimal preparation of Pt/TiO_2 photocatalysts using atomic layer deposition, Appl. Catal. B: Environ. 101 (2010) 54–60.
[30] Y. Zhou, C.L. Muhich, B.T. Neltner, A.W. Weimer, C.B. Musgrave, Growth of Pt particles on the anatase TiO_2 (101) surface, J. Phys. Chem. C 116 (2012) 12114–12123.
[31] S. Zhuiykov, T. Kawaguchi, Z. Hai, M.K. Akbari, P.M. Heynderickx, Interfacial engineering of two-dimensional nano-structured materials by atomic layer deposition, Appl. Surf. Sci. 392 (2017) 231–243.
[32] H. Azizpour, R. Sotudeh-Gharebagh, N. Mostoufi, R. Zarghami, Characterization of regime transition in fluidized beds at high velocities by analysis of vibration signals, Ind. Eng. Chem. Res. 51 (2012) 2855–2863.
[33] J. Shabanian, R. Jafari, J. Chaouki, Fluidization of ultrafine powders, Int. Rev. Chem. Eng. 4 (2012) 16–50.
[34] M. Shiea, R. Sotudeh-Gharebagh, H. Azizpour, N. Mostoufi, R. Zarghami, Predicting transition velocities from bubbling to turbulent fluidization by S-statistics on vibration signals, Part. Sci. Technol. 31 (2013) 10–15.
[35] M. Tahmasebpoor, L. de Martín, M. Talebi, N. Mostoufi, J.R. van Ommen, The role of the hydrogen bond in dense nanoparticle–gas suspensions, Phys. Chem. Chem. Phys. 15 (2013) 5788–5793.
[36] M.R. Tamadondar, R. Zarghami, H. Azizpour, N. Mostoufi, J. Chaouki, R. Radmanesh, Using S-statistic for investigating the effect of temperature on hydrodynamics of gas–solid fluidization, Particuology 11 (2013) 288–293.
[37] T. Vaidya, Fluidization behavior of alumina nano-Particles, in: Applied Mechanics and Materials, Trans Tech Publ, 2012, pp. 1833–1840.
[38] J.R. van Ommen, J.M. Valverde, R. Pfeffer, Fluidization of nanopowders: a review, J. Nanopart. Res. 14 (2012) 1–29.
[39] W. Yao, G. Guangsheng, W. Fei, W. Jun, Fluidization and agglomerate structure of SiO_2 nanoparticles, Powder Technol. 124 (2002) 152–159.
[40] L. Zhou, H. Wang, T. Zhou, K. Li, H. Kage, Y. Mawatari, Model of estimating nano-particle agglomerate sizes in a vibro-fluidized bed, Adv. Powder Technol. 24 (2013) 311–316.
[41] M. Tamadondar, H. Azizpour, R. Zarghami, N. Mostoufi, J. Chaouki, Using particle trajectory for determining the fluidization regime in gas–solid fluidized beds, Adv. Powder Technol. 23 (2012) 349–351.
[42] J. Ferguson, A. Weimer, S. George, Atomic layer deposition of Al_2O_3 and SiO_2 on BN particles using sequential surface reactions, Appl. Surf. Sci. 162 (2000) 280–292.
[43] J. Ferguson, A. Weimer, S. George, Atomic layer deposition of SiO_2 films on BN particles using sequential surface reactions, Chem. Mater. 12 (2000) 3472–3480.
[44] J. Ferguson, A. Weimer, S. George, Atomic layer deposition of boron nitride using sequential exposures of BCl_3 and NH_3, Thin Solid Films 413 (2002) 16–25.
[45] J. Ferguson, A. Weimer, S. George, Surface chemistry and infrared absorbance changes during ZnO atomic layer deposition on ZrO_2 and $BaTiO_3$ particles, J. Vacuum Sci. Technol. A 23 (2005) 118–125.
[46] V. Miikkulainen, M. Leskelä, M. Ritala, R.L. Puurunen, Crystallinity of inorganic films grown by atomic layer deposition: overview and general trends, J. Appl. Phys. 113 (2013) 021301.
[47] L.F. Hakim, C.L. Vaughn, H.J. Dunsheath, C.S. Carney, X. Liang, P. Li, A.W. Weimer, Synthesis of oxidation-resistant metal nanoparticles via atomic layer deposition, Nanotechnology 18 (2007) 345603.
[48] X. Liang, D.M. King, M.D. Groner, J.H. Blackson, J.D. Harris, S.M. George, A.W. Weimer, Barrier properties of polymer/alumina nanocomposite membranes fabricated by atomic layer deposition, J. Membr. Sci. 322 (2008) 105–112.
[49] X. Liang, A.D. Lynn, D.M. King, S.J. Bryant, A.W. Weimer, Biocompatible interface films deposited within porous polymers by atomic layer deposition (ALD), ACS Appl. Mater. Interfaces 1 (2009) 1988–1995.
[50] P. Lichty, X. Liang, C. Muhich, B. Evanko, C. Bingham, A.W. Weimer, Atomic layer deposited thin film metal oxides for fuel production in a solar cavity reactor, Int. J. Hydrogen Energy 37 (2012) 16888–16894.
[51] B. Moghtaderi, I. Shames, E. Doroodchi, Combustion prevention of iron powders by a novel coating method, Chemical Eng. Technol. 29 (2006) 97–103.
[52] R. Beetstra, J. Nijenhuis, E.M. Kelder, J.R. van Ommen, Improved Li-ion battery performance by coating cathode nano-particles using atomic layer deposition, 2007.
[53] Z. Zhou, N. Zhou, X. Lu, M. ten Kate, D. Valdesueiro, J.R. van Ommen, H.B. Hintzen, Performance improvement by alumina coatings on $Y_3Al_5O_{12}$: Ce^{3+} phosphor powder deposited using atomic layer deposition in a fluidized bed reactor, RSC Adv. 6 (2016) 76454–76462.
[54] D. Valdesueiro, M.K. Prabhu, C. Guerra-Nunez, C.S. Sandeep, S. Kinge, L.D. Siebbeles, L.C. de Smet, G.M. Meesters, M.T. Kreutzer, A.J. Houtepen, Deposition mechanism of aluminum oxide on quantum dot films at

atmospheric pressure and room temperature, J. Phys. Chem. C 120 (2016) 4266–4275.
[55] D. Valdesueiro, P. Garcia-Triñanes, G. Meesters, M. Kreutzer, J. Gargiuli, T. Leadbeater, D. Parker, J. Seville, J. van Ommen, Enhancing the activation of silicon carbide tracer particles for PEPT applications using gas-phase deposition of alumina at room temperature and atmospheric pressure, Nucl. Instrum. Methods Phys. Res., Sect. A 807 (2016) 108–113.
[56] M.N. Mirvakili, H. Van Bui, J.R. van Ommen, S.G. Hatzikiriakos, P. Englezos, Enhanced barrier performance of engineered paper by atomic layer deposited Al_2O_3 thin films, ACS Appl. Mater. Interfaces 8 (21) (2016) 13590–13600.
[57] A. Philip, S. Thomas, K.R. Kumar, Calculation of growth per cycle (GPC) of atomic layer deposited aluminium oxide nanolayers and dependence of GPC on surface OH concentration, Pramana 82 (2014) 563–569.
[58] M.B.M. Mousa, C.J. Oldham, G.N. Parsons, Atmospheric pressure atomic layer deposition of Al_2O_3 using trimethyl aluminum and ozone, Langmuir 30 (2014) 3741–3748.
[59] D.N. Goldstein, J.A. McCormick, S.M. George, Al_2O_3 atomic layer deposition with trimethylaluminum and ozone studied by in situ transmission FTIR spectroscopy and quadrupole mass spectrometry, J. Phys. Chem. C 112 (2008) 19530–19539.
[60] J.R. Wank, S.M. George, A.W. Weimer, Coating fine nickel particles with Al_2O_3 utilizing an atomic layer deposition-fluidized bed reactor (ALD–FBR), J. Am. Ceram. Soc. 87 (2004) 762–765.
[61] M. Groner, F. Fabreguette, J. Elam, S. George, Low-temperature Al_2O_3 atomic layer deposition, Chem. Mater. 16 (2004) 639–645.
[62] A. Ott, J. Klaus, J. Johnson, S. George, Al_2O_3 thin film growth on Si (100) using binary reaction sequence chemistry, Thin Solid Films 292 (1997) 135–144.
[63] M. Leskelä, M. Ritala, Atomic layer deposition chemistry: recent developments and future challenges, Angew. Chem. Int. Ed. 42 (2003) 5548–5554.
[64] V.R. Rai, V. Vandalon, S. Agarwal, Influence of surface temperature on the mechanism of atomic layer deposition of aluminum oxide using an oxygen plasma and ozone, Langmuir 28 (2011) 350–357.
[65] M. Rose, J. Niinistö, I. Endler, J.W. Bartha, P. Kücher, M. Ritala, In situ reaction mechanism studies on ozone-based atomic layer deposition of Al_2O_3 and HfO_2, ACS Appl. Mater. Interfaces 2 (2010) 347–350.
[66] J. Spiegleman, J. Sundqvist, Comparison of water vapor to ozone for growth of ALD Films, in: Conference poster paper, PVSEC 2011, Hamburg, Germany, 2011.
[67] C.L. Duan, X. Liu, B. Shan, R. Chen, Fluidized bed coupled rotary reactor for nanoparticles coating via atomic layer deposition, Rev. Sci. Instrum. 86 (2015) 075101.
[68] X. Xiao, G. Cao, F. Chen, Y. Tang, X. Liu, W. Xu, Durable superhydrophobic wool fabrics coating with nanoscale Al_2O_3 layer by atomic layer deposition, Appl. Surf. Sci. 349 (2015) 876–879.
[69] M. Juppo, A. Rahtu, M. Ritala, In situ mass spectrometry study on surface reactions in atomic layer deposition of TiN and Ti (Al) N thin films, Chem. Mater. 14 (2002) 281–287.
[70] A.H. Harvey, E.W. Lemmon, Correlation for the vapor pressure of heavy water from the triple point to the critical point, J. Phys. Chem. Ref. Data 31 (2002) 173–181.
[71] S. Elliott, G. Scarel, C. Wiemer, M. Fanciulli, G. Pavia, Ozone-based atomic layer deposition of alumina from TMA: Growth, morphology, and reaction mechanism, Chem. Mater. 18 (2006) 3764–3773.
[72] S.D. Elliott, J.C. Greer, Simulating the atomic layer deposition of alumina from first principles, J. Mater. Chem. 14 (2004) 3246–3250.
[73] D.M. King, A.W. Weimer, Titanium dioxide particles coated via an atomic layer deposition process, Google Patents, 2012.
[74] F.H. Saboor, T. Ueda, K. Kamada, T. Hyodo, Y. Mortazavi, A.A. Khodadadi, Y. Shimizu, Enhanced NO_2 gas sensing performance of bare and Pd-loaded SnO_2 thick film sensors under UV-light irradiation at room temperature, Sens. Actuators, B 223 (2016) 429–439.
[75] D.C.L. Vasconcelos, E.H.M. Nunes, M. Gasparon, W.L. Vasconcelos, Infrared spectroscopy of titania sol-gel coatings on 316L stainless steel, Materials Sciences and Applications 2 (2011) 1375.